Applied Geochemistry 137 (2022) 105203

Contents lists available at ScienceDirect

Applied Geochemistry

journal homepage: www.elsevier.com/locate/apgeochem

Pyrite oxidation by nitrate and nitrite in sodium bicarbonate solution under anoxic and abiotic conditions

Katrien Hendrix [a,*], Nele Bleyen [a], Thierry Mennecart [a], Pierre Eloy [b], Eric M. Gaigneaux [b], Elie Valcke [a]

[a] Expert Group Waste & Disposal, SCK CEN, Boeretang 200, 2400, Mol, Belgium
[b] Institute of Condensed Matter and Nanosciences (IMCN), UCLouvain, Place Louis Pasteur, 1, Box L4.01.09, 1348, Louvain-la-Neuve, Belgium

ARTICLE INFO

Editorial handling by Thomas Gimmi

Keywords:
Pyrite
Boom clay
Nitrate
Nitrite
Geochemistry
Anoxic conditions
Abiotic conditions
Geological disposal

ABSTRACT

Pyrite reactivity with nitrate and nitrite was assessed in long-term batch tests to assess its possible oxidation in anoxic conditions at pH 8.5, at room temperature and atmospheric pressure. This was done in the frame of compatibility studies of nitrate-containing radioactive waste with a pyrite-containing clay host rock for geological disposal. Abiotic pyrite suspensions were prepared under inert atmosphere in 15 mM bicarbonate medium, as this simulates the inorganic carbon and pH conditions in the pore water of Boom Clay, which is a potential host rock for geological disposal in Belgium. Two forms of pyrite powder were used, formed via different genetic pathways and exhibiting a different morphology, namely pyrite obtained by crushing a large crystal cluster and pyrite extracted from Boom Clay by flotation. The reactivity of these two pyrite forms with nitrate and nitrite is reported and compared. Overall, after 2–2.5 years under abiotic conditions and inert atmosphere, no significant reaction between crushed pyrite and nitrate was detected, while a very limited reaction was observed between Boom Clay pyrite and nitrate. Between pyrite and nitrite, which is known to be more reactive than nitrate, a slow reaction took place for both forms of pyrite, with no significantly higher reactivity with the Boom Blay pyrite. The variability between the replicates of Boom Clay pyrite were also larger than for crushed pyrite. Overall, nitrate and nitrite induced a very limited, if any, oxidation reaction of the pyrite powders. These observations are important in assessing the safety of geological disposal of nitrate-containing radioactive waste.

1. Introduction

Waste forms with high nitrate content are often considered problematic. Indeed, nitrate is a readily soluble and highly mobile component that can be quite reactive as oxidant. Methods such as biological remediation are often applied to remove the nitrate from e.g. municipal wastewater streams (Flere and Zhang, 1998; Hunter and Shaner, 2010; Jordan et al., 2008). The research described in this paper is dealing with Eurobitum, a nitrate-containing radioactive waste consisting mainly of a Mexphalt bitumen matrix (~60 wt%) with large amounts of $NaNO_3$ (20–30 wt%). Since the presence of radionuclides makes (bio-)remediation much more difficult (or even impossible) and expensive, removing the nitrate is not considered here. Therefore, rather than removing the nitrates from the waste, their impact on the proposed waste disposal system and surroundings is being studied.

For Eurobitum, being one of the important intermediate-level long-lived radioactive waste (ILW) forms in Belgium, the option currently considered is geological disposal in a poorly indurated clay. After disposal, water from the surrounding clay will infiltrate the engineered barrier system and will come in contact with the Eurobitum, over time dissolving the $NaNO_3$. Subsequently, leaching of nitrate and to a lesser extent nitrite (formed by radiolytic and/or (bio)chemical nitrate reduction (Bleyen et al., 2018a)) out of the waste drums and into the surrounding host rock will occur.

Boom Clay is currently considered as a potential host rock for geological disposal of ILW in Belgium. It has interesting physico-chemical properties, which will cause a delay and spread in time of the migration of leached radionuclides. One of these properties is the reducing environment of the Boom Clay, imposed by the presence of redox-active species, *i.e.* mainly pyrite from the mineral phase and dissolved organic matter and kerogen from the organic phase. The reducing nature of the Boom Clay is an important asset to limit the mobility of

* Corresponding author.
E-mail address: khendrix@sckcen.be (K. Hendrix).

https://doi.org/10.1016/j.apgeochem.2022.105203
Received 10 September 2021; Received in revised form 22 December 2021; Accepted 7 January 2022
Available online 11 January 2022
0883-2927/© 2022 Elsevier Ltd. All rights reserved.

redox-sensitive radionuclides leaching from Eurobitum (Bruggeman and Maes, 2017). Indeed, a more oxidized Boom Clay environment would lead to more radionuclides remaining in their oxidized state, which are in general more mobile than in their reduced state (De Cannière et al., 2010). As besides radionuclides nitrate (and in lesser amounts also nitrite) will leach from Eurobitum, it is thus important to investigate the impact of nitrate (and nitrite) on the reducing capacity of Boom Clay and more specifically on its redox-active species such as pyrite.

Oxic pyrite oxidation has been studied extensively in the past, since this causes significant acidification in soils and aquifers (Golez and Kyuma, 1997; Evangelou, 1995). It is well documented in mining industry as well as in brackish water aquaculture. When exposed to air, pyrite is oxidized by oxygen, leading to the precipitation of ferric oxy-hydroxides and to the release of sulfuric acid in water (Golez and Kyuma, 1997). Baeyens et al. have reported the air exposure of Boom Clay, in which pyrite oxidation played the main role and the effect of this oxidation was similar to acid sulfate soils (Baeyens et al., 1985). Indeed, complete pyrite oxidation generated a very strong acidity due to the formation of sulfuric acid, causing the dissolution of $CaCO_3$ and progressive aluminization of the Boom Clay.

Chemolithoautotrophic microbial denitrification coupled to pyrite oxidation at circumneutral pH has also been studied quite extensively, to various outcomes. This bioprocess is promising for removal of nitrate from groundwater of wastewater. However, research on this anaerobic pyrite oxidation with nitrate as electron acceptor has yielded different results depending on the experimental protocols applied. Interference with impurities in the pyrite such as Fe(III) and elemental sulfur have led to overestimations of the pyrite oxidation by denitrification (Yan et al., 2021). The properties of the pyrite were also important, for example pure crystalline pyrite did not react with nitrate, while oxidation by denitrification of lab-synthesized FeS_2 of low crystallinity was possible according to Yan et al. (2019).

Thiobacillus cultures are the most commonly applied biogeochemical systems to study microbial denitrification coupled to pyrite oxidation, with *Thiobacillus denitrificans* as the most prominent chemolithoautotrophic model organism for conserving energy from the oxidation of inorganic sulfur compounds coupled to denitrification (Golez and Kyuma, 1997; Bosch et al., 2012; Jørgensen et al., 2009; Vaclavkova et al., 2015), although *Acidovorax* has also been studied (Klueglein and Kappler, 2013). Overall, microbial reduction of nitrate by pyrite appears to be induced via S oxidation but not via Fe oxidation.

Other studies on the abiotic, chemical reduction of nitrate can be found as well, for example Buresh and Moraghan studied the reduction by ferrous ion, in a pH range of 6–10, where it was found that nitrate could indeed be reduced by ferrous ion in the presence of Cu^{2+} (Buresh and Moraghan, 1976). However, the abiotic, purely chemical oxidation of pyrite by nitrate or nitrite has either not yet been assessed or bacterial inhibitors such as NaN_3 were added, which may have perturbed the results (Jørgensen et al., 2009; Hendrix et al., 2019). A long-term study, spanning multiple years, of the anoxic and abiotic reactivity of pyrite with nitrate and nitrite at room temperature and atmospheric pressure has not yet been reported to the knowledge of the authors.

As part of the ongoing compatibility study of Eurobitum with geological disposal in Boom Clay, a possible abiotic and biotic reaction of Boom Clay with nitrate and nitrite at a pH of 8.5, representative of the Boom Clay pore water pH (?), is assessed. To this end, several series of batch tests were conducted at SCK CEN in a parametric approach to study the individual reactivity of the Boom Clay components. This paper discusses a possible pyrite oxidation by nitrate or nitrite in a simplified proxy of real Boom Clay pore water, to decouple the reactivity of other components in the pore water (mostly dissolved organic matter) from the reactivity of pyrite, which is under investigation here. Two forms of pyrite were used in the tests, one was obtained by crushing commercially available, euhedral pyrite in the form of a large block, and the other was extracted by flotation from Boom Clay, with a euhedral and framboidal morphology. This research compares the reactivity of both forms of pyrite with nitrate and nitrite under abiotic conditions.

2. Materials and methods

2.1. Pyrite

Two forms of pyrite were used in the presented tests. The first form of pyrite is formed through precipitation in a reducing, sulfate-rich environment (Imai et al., 1985). Its macrostructural morphology is a cubic rock, which was obtained from Alfa Aesar (VWR) as a crystal cluster and by-product from Peruvian mines. It was crushed into a powder according to the procedure in Section 2.1.1 and is further referred to as 'crushed pyrite'. The second form of pyrite was formed in situ by sulfate-reducing bacteria, which reduce sulfate ions to sulfide in the presence of iron, forming pyrite. It has a mainly framboidal morphology (Wilkin and Barnes, 1997). It was extracted from Boom Clay, as explained in Section 2.1.2 and is therefore further referred to as 'Boom Clay pyrite'.

2.1.1. Crushed pyrite from large crystal cluster

A pyrite crystal cluster stemming from a Peruvian mine (VWR, US) was first crushed with a hammer and treated with 37 wt% HCl to remove the outer oxidized layer. This treatment was done under a fume hood. Upon breaking the pyrite crystal cluster with a hammer, it fell apart into small fractions. These pyrite lumps (~1 cm^3 in size) were placed in several glass 100 mL recipients containing a 37 wt% HCl solution and closed off with a lid. Every 20 min, it was verified whether there was still pyrite left in the solution, since HCl not only removes the outer most oxidized layer, but also dissolves the pyrite itself. The pyrite lumps remained largely intact and were therefore kept in HCl solution during 1 h. The pyrite was filtered over a 150 μm glass filter to remove the HCl. After filtration, the pyrite lumps were immediately transferred to a glass recipient, covered with ethanol and closed with a lid. This recipient was brought into the glovebox ($[O_2] < 1$ ppm). In the glovebox, the ethanol was decanted first and then filtered off with a 150 μm glass filter. This washing step with ethanol was repeated a few times until the ethanol no longer showed any discoloration. The pyrite was left to dry in the glovebox. It was then transferred to the ball mill recipient that was brought into the glovebox, an agate box with lid and seven agate balls inside. The ball mill lid was taped to the box with electrical tape to limit the inflow of O_2. It was then brought out of the glovebox for milling during 30 min at speed 400 rpm in a Centrifugal Ball Mill Type S 100 (Retsch, Germany). After milling, the ball mill recipient was brought into the glovebox again and opened. The pyrite was removed with a spatula and brush and this time sieved over a 125 μm mesh size sieve, while manually shaking. The pyrite powder was transferred to septum bottles, again submerged in ethanol and capped with a septum lid. It was then placed in a sonication bath outside the glovebox during 30 min. The pyrite was again brought back into the glovebox to remove the ethanol (decanted and filtered over 125 μm filter paper). The pyrite was lastly dried overnight, on the filter paper, in the glovebox.

2.1.2. Pyrite extracted from Boom Clay

Pyrite was extracted from a block of Boom Clay, obtained from a Boom Clay sample taken from the Putte member during the excavation of the connecting gallery in the URL on February 20th and 27th 2002 (SCK-CEN, 2020; Delécaut, 2004). To prevent possible oxidation by oxygen, the sample was immediately packed under vacuum in aluminum-coated polyethylene sheets and stored in a dark cold room at 6 °C. The extraction of pyrite from Boom Clay was done in March 2002 by the Centre Terre et Pierre (CTP, Tournai, Belgium). It involved multiple steps with a final flotation step in which a surfactant, in this case Dowfroth™ 250, a polyol produced by DOW chemicals, was added. The surfactant adhered to the pyrite, bringing it to the top of the suspension, from where it could be removed, as described in the patent by Miller (1974). The steps taken to extract the pyrite were:

1. Crumbling of Boom Clay in water;
2. Sieving to retain <1.25 mm fraction;
3. Gravimetric separation by Knelson concentrator (20 kPa counter pressure);
4. Gravimetric separation by Knelson concentrator (10 kPa counter pressure);
5. Light fraction retained;
6. Separation of coarse and fine fraction by hydrocyclone;
7. Second separation of coarse fraction by hydrocyclone;
8. Flotation with surfactant (Dowfroth™ 250);
9. Pyrite is retained as floating phase;
10. Pyrite is cleaned by multiple washing steps with deionized water and ethanol to remove the surfactant.

The pyrite was stored in the glovebox at SCK CEN. Before use in the presented batch tests, the powder was washed. This was done in the glovebox by immersing the pyrite powder in deionized water in a septum bottle. This was capped, brought out of the glovebox and put in an ultrasonic bath during 1 h, after which it was brought back into the glovebox. The water was decanted inside the glovebox. This was repeated three times. The pyrite was then taken out of the glovebox and treated with 37% HCl to remove the outer oxidized layers. This was done in the same way as for the crushed pyrite. In short, the pyrite extracted from Boom Clay was:

- Immersed in 37 wt% HCl during 1 h;
- HCl solution was removed by filtrating the suspension over a 150 μm filter;
- The pyrite was submerged in ethanol and brought into the glovebox ([O2] < 1 ppm);
- The pyrite in ethanol suspension was sonicated during 30 min;
- The ethanol was removed by filtration over a 150 μm filter;
- The pyrite was washed three more times with ethanol in the glovebox until the ethanol did not show any more discoloration and subsequently left to dry.

2.2. Aqueous phase

A 15 x 10^{-3} M $NaHCO_3$ solution was obtained by dissolving 1.26 g of $NaHCO_3$ (VWR) per liter deionized water in the anaerobic glovebox (N_2 or argon atmosphere, $[O_2] < 5$ ppm). This bicarbonate concentration was chosen to mimic the in situ TIC concentration and pH of Boom Clay pore water, which is about 8.5. Different concentrations of $NaNO_3$ or $NaNO_2$ were added to these solutions by weighing the necessary amount of powder and adding it to the bicarbonate solutions in the glovebox, as indicated in Table 1.

In some cases, the bicarbonate solution was filtered to remove possible microbial contamination. More information can be found in Section 2.3.

2.3. Test setup

Pyrite suspension were prepared in a 15 x 10^{-3} M sodium bicarbonate solution in the anaerobic glovebox (N_2 or argon atmosphere, $[O_2] < 5$ ppm). This bicarbonate solution was used as a proxy of real Boom Clay pore water, having a pH of around 8.5 and TIC (total inorganic carbon) concentration similar to the real Boom Clay pore water. As maximum concentration, 0.1 M nitrate was chosen, based on scoping calculations suggesting that nitrate could reach a concentration of 0.1 M at a distance of 5 m from the disposal gallery interface (Weetjens et al., 2006). A nitrate concentration of 0.005 M was also applied for crushed pyrite to verify the overall impact of concentration on reactivity (if any). This was not done for Boom Clay pyrite due to a limited availability of this pyrite powder. Nitrite is only expected as a (radiolytic and biochemical) reduction product of nitrate and therefore its concentration is expected to be lower and was set to 0.005 M (crushed pyrite) or 0.05 M (pyrite extracted from Boom Clay).

Table 1
Overview of all test conditions. *Rep. stands for the code of the replicate series. For no.1, no replicate was prepared.

No.	Rep. *	Pyrite type	Atmosphere	$NaNO_3$ (M)	$NaNO_2$ (M)	Sampling times (days)
1	/	Crushed	N_2	0	0	0, 35, 91, 183, 364, 924
2	a	Crushed	N_2	0.1	0	0, 35, 91, 183, 364, 924
3	b	Crushed	N_2	0.1	0	0, 35, 91, 183, 364, 924
4	a	Crushed	N_2	0.005	0	0, 183, 924
5	b	Crushed	N_2	0.005	0	0, 183, 924
6	a	Crushed	N_2	0	0.005	0, 29, 91, 182, 351, 924
7	b	Crushed	N_2	0	0.005	0, 29, 91, 182, 351, 924
8	a	Boom Clay	Ar	0	0	2, 28, 85, 182, 364, 741
9	b	Boom Clay	Ar	0	0	2, 28, 364, 741
10	a	Boom Clay	Ar	0.1	0	2, 28, 85, 182, 364, 741
11	b	Boom Clay	Ar	0.1	0	2, 28, 364, 741
12	a	Boom Clay	Ar	0	0.05	2, 28, 85, 182, 364, 741
13	b	Boom Clay	Ar	0	0.05	2, 28, 364, 741

Table 1 gives an overview of all test conditions. Two replicate series ('a' and 'b') were prepared for each test condition and most sampling times, as indicated in the table. At each sampling time, a replicate was sacrificed.

Amber-colored 110 mL septum bottles were filled with 0.35 g pyrite powder and 70 mL bicarbonate solution, with and without various concentrations of nitrate and nitrite, as indicated in Table 1. The septum bottles were filled in a glovebox under inert atmosphere and stored there during the experiment. Care was taken to avoid any contamination by oxygen, which could oxidize the pyrite surface. Moreover, additional steps were taken to avoid nitrogen in the glovebox under argon atmosphere (test no. 8 to 13), since nitrogen gas generation was to be followed up in these septum bottles. To this end, all materials were brought into the glovebox through a lock that was thoroughly rinsed three times to remove oxygen and nitrogen by introducing a vacuum and 100% argon at atmospheric pressure. The materials were then allowed to come into full equilibrium with the argon atmosphere in the glovebox overnight.

For all test conditions, abiotic conditions were demonstrated with most probably number (MPN) and/or adenosine triphosphate (ATP) concentration analyses (methods according to Bleyen et al. (2016)) throughout the experiment. These tests give an insight in the possible microbial growth (MPN) and activity (ATP) present in the samples. The MPN analysis is a statistical method based on the random dispersion of microorganisms per volume in a given sample. In this method, measured volumes of water are added to a series of tubes containing a liquid indicator growth medium. The ATP concentration, which is the energy-carrying molecule in all living cells, gives an indication on how large and active a microbial community is. For tests no. 10 and 11, the bicarbonate solution was filter sterilized using a Supor® polysulfone filter with a 0.2 μm pore size prior to addition of the pyrite powder, to remove bacterial contamination. This was deemed necessary after an initial batch test with non-sterilized solution was perturbed by microbial activity. The MPN and ATP analysis results (supplementary information) confirm abiotic conditions in all presented batch tests.

2.4. Analysis methods

2.4.1. Gas phase analysis

The gas phase in the headspace was sampled by piercing the septum with a needle connected to a gas container under vacuum. The pressure in the headspace before sampling was calculated based on the volumes of the headspace and gas container and on the gas pressure in the container after sampling. Analysis of the N_2 and N_2O concentration was performed by Hydroisotop (Schweitenkirchen, Germany) by gas chromatography (QMA 504-2/15 column) coupled with a Thermal Conductivity Detector or in-house by μGas Chromatography (PoraPLOT U column) combined with a Thermal Conductivity Detector (Varian CP-4900 Micro GC). For the test conditions 1–7 (Table 1), N_2 production could not be detected due to the presence of N_2 in the septum bottles at the start of the test (N_2 = gas atmosphere in abiotic glove box). The concentrations of the dissolved gas in the solution were calculated with Henry's law by multiplying the partial pressure (from the total measured pressure) with the Henry coefficient constant for N_2O (2.3×10^{-2} M/atm) or for N_2 (6.1×10^{-4} M/atm) (Sander, 2015).

2.4.2. Aqueous phase analysis

Chemical analyses were performed on the supernatant of the pyrite suspensions after settling of the pyrite. To prevent perturbation of the chemical analyses by small pyrite particles, the supernatant was additionally filtered over a Supor® polysulfone filter with a 0.2 μm pore size.

The concentrations of NO_3^-, NO_2^-, SO_4^{2-} and $S_2O_3^{2-}$ were analyzed at Lovap research lab (Geel, Belgium), by Ion Chromatography (or IC; DX600, Dionex Thermo, Dionex Ion Pac AS4A-SC). The total iron in solution was measured by Lovap research lab (Geel, Belgium) by inductively coupled plasma atomic emission spectroscopy (or ICP-AES; Agilent 5800 VDV). TOC/TIC measurements were performed in-house with a TOC/TIC analyzer using the combustion and acidification method. The pH measurements were done with a Mettler-Toledo pH electrode, which was calibrated before each use with fresh pH buffers 7 and 10.

2.4.3. Pyrite analysis techniques

The pyrite powders were analyzed before the batch tests were started and at the end of the tests (2 years for Boom Clay pyrite, 2.5 years for crushed pyrite). They were prepared in the glovebox after sampling of the solution (see Section 2.4.2). To prevent salt deposition on the pyrite surface during drying, 100 mL of deionized water was added to the septum bottles. The pyrite was left to settle, after which the water was decanted. In a next step, ethanol was added to the pyrite suspension and again removed by decanting it after the pyrite had settled. This step with ethanol was repeated. Afterwards, the wet pyrite was left to dry in the glovebox ($[O_2] < 5$ ppm). Once fully dry (at least 1 week), the septum bottles with pyrite powder were capped, brought outside the glovebox and stored in a desiccator.

X-ray diffraction analysis (XRD) was done with a Philips X'Pert Diffractometer equipped with a Cu-Kα tube at 45 kV and 40 mA. Measurement temperature was 25 °C, measured over a 2θ range of 20–120° with a divergence slit size of 0.5°. The data were analyzed with the X'Pert HighScore Plus software with accompanying database. Reference patterns were calculated by the software from ICSD using POWD-12++, (1997).

Scanning Electron Microscopy coupled with Energy-dispersive X-ray spectroscopy (SEM-EDX) was performed with a JEOL (JSM 6610) with Bruker software. The working distance of the microscope stage was 10 mm, with a stage height of 10 mm. Secondary electron imaging (SEI) was used at a voltage of 15 kV. SEM images and EDX analysis were taken from at least three different spots for each sample.

BET specific surface area analysis (based on the Brunauer, Emmett and Teller theory) was done using N_2 as the adsorbent. These N_2 adsorption measurements were done on pyrite powder with a TriStar II 3020 Micromeritics. The specific surface area was measured at least in threefold on three individual samples.

The pyrite samples were analyzed by X-ray photoelectron spectroscopy (XPS) after the final sampling (2–3 years after start). Pyrite powder samples were placed on carbon tape and brought into the XPS chamber and put under high vacuum. The XPS measurements were obtained using a VG Scientific Escalab 220i-XL. The analyses were realized with a monochromatic Al Kα X-ray source (1486.6 eV), operated at 15 kV and 150 W. The analyzed surface was in the order of 500 x 500 μm^2. The XPS spectra were analyzed using the Thermo Electron Advantage® software with continuous background subtraction according to the Shirley model (Végh, 2006). Large survey spectra were recorded over the 0–1200 eV range in order to determine the composition of the surface. Using the analytical software, their atomic percentages were estimated by integrating the peak area with Scofield sensitivity factors as defined in the software package. Based on the large survey and the identification of the main compounds, high-resolution narrow spectra were recorded in the valence band regions of Fe2p, S2p, C1s, O1s and Fe3p. The Fe3p spectra were larger than the Fe3p peak itself in order to catch also the Si2p, Al2s and Br3d. A correction was systematically applied using the main peak C1s attributed to adventitious carbon at 285.0 eV. This value is commonly used to correct the energy shift of the scan because of the charging effect. Note that XPS is a technique that probes the surface of a material to a depth of about 5 nm and has an uncertainty of 20–30%. The shown XPS results are only part of the spectra, in two regions of binding energy. From 700 to 725 eV, the Fe $2p_{3/2}$ photoelectron peak is found, attributed to, among other iron species, $FeSO_4$, $FeCO_3$ and pyrite. The Fe 2p peak showed a well-resolved $2p_{3/2}$ - $2p_{1/2}$ doublet in all measurements, which is why only the Fe $2p_{3/2}$ is discussed. Around 160 eV, the S $2p_{3/2}$ and S $2p_{1/2}$ photoelectron peaks are found, thus related to the sulfur-species on the surface. Again, the spectra were compared by normalizing the total peak surface area. The sulfur species present at the surface were compared qualitatively in this way.

3. Results and discussion

3.1. Characterization of the pyrite starting materials

3.1.1. Morphology by SEM-EDX

The morphology of the two types of pyrite is shown in the SEM images in Fig. 1.

For the pyrite obtained by crushing of the large crystal, it was found that the pyrite grains are rather irregular in appearance and their surface was coated with small particles. Milling of the large cubic block of pyrite thus led to pyrite fractions in different shapes. The larger grains were roughly 100 μm in size while others were merely 1 μm. Similar results were obtained by laser diffraction analysis (supplementary information). Since this material was sieved with a 125 μm mesh size, this was to be expected. The small particles coating the surface were nanoparticles in size. This is likely due to the crushing and milling, the sonication steps in ethanol apparently did not remove all nanoparticles (see Section 2.1.1 for the preparation procedure). The larger pyrite grains are irregular in appearance and vary in size; their surface is uneven and appear to be resulting from conchoidal fractures. This is to be expected since pyrite lacks preferential cleavage plains (Nesbitt et al., 1998), thus these irregular shapes are a direct result from the crushing and milling. EDX results showed that about 1 at% of Si was present in the samples, while S and Fe made up most of the material. Some O and C was also found. It is thus likely that some of the small particles observed are silica. This can be a result of the agate (SiO_2) materials milling in the agate ball and mill jar. However, the silicium oxide present on the pyrite is not expected to be reactive in the presented setups and should not cause experimental artefacts. The at% ratio of Fe to S from EDX results, based on eight point-measurements on a flat surface of pyrite (not a nano-sized grain), was 0.6 ± 0.1, so slightly more Fe was present than can be expected from the FeS_2 stoichiometry of pyrite (theoretical Fe/S at% ratio = 0.5).

The Boom Clay pyrite had a different morphology from the crushed

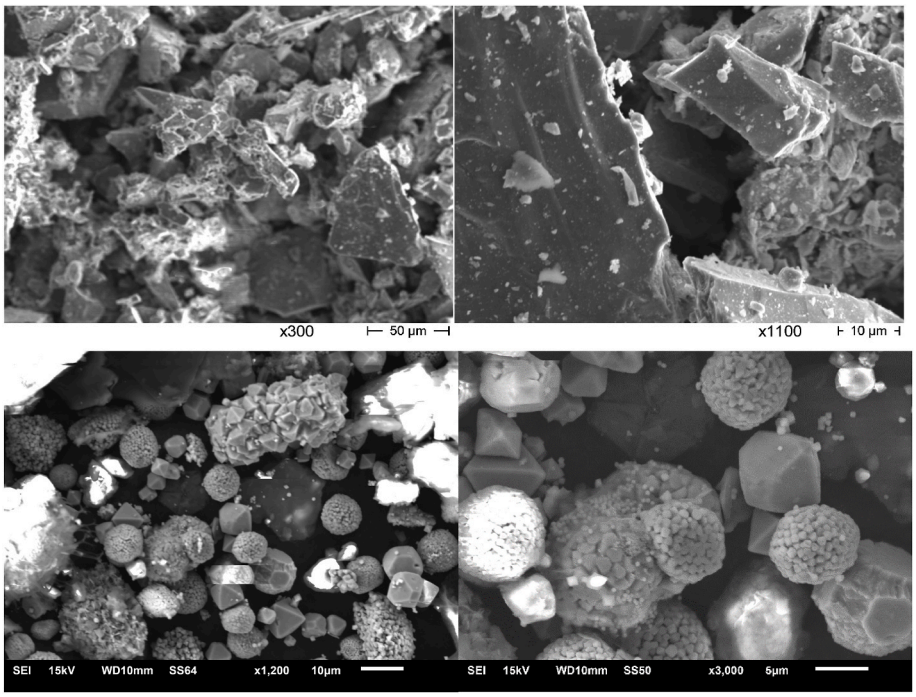

Fig. 1. SEM image of crushed pyrite from a large pyrite crystal cluster (top) and Boom Clay pyrite (bottom). The magnification and scale are indicated at the bottom of the images.

pyrite. Some of the pyrite was cubic in form, consisting of small cubic crystals of about 5 µm size, while a large part was framboidal. Framboidal pyrite typically consists of very small spheres of euhedral pyrite crystals, most often cubic pyrite crystals of about 1 µm composed into a sphere of about 10 µm. The Boom Clay pyrite was not crushed, milled and sieve like the crushed pyrite (Fig. 1, top images), which can also explain its different appearance and absence of very small fragments. No Si was observed with SEM-EDX, which was also different from the crushed pyrite, likely because it was not milled in an agate ball and mill. This framboidal morphology is found in many anoxic environments, of which argillaceous marine sediments such as the Boom Clay are examples (Wilkin and Barnes, 1997). Its origin is assumed pyritic fossilization

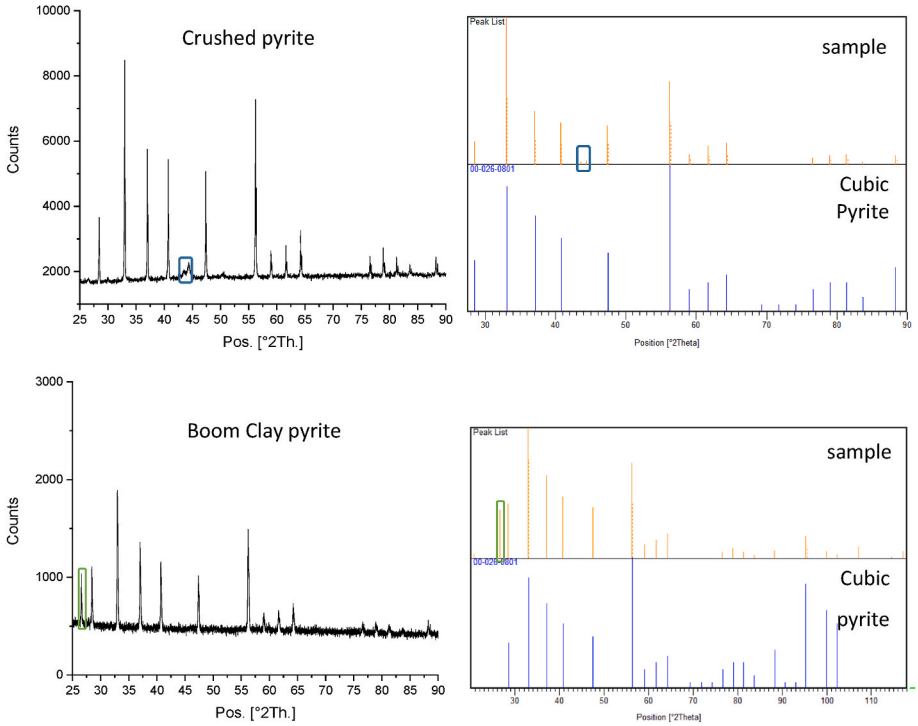

Fig. 2. XRD diffractogram (left) and reflection pattern (right) of the pyrite powders. The XRD reflection pattern of the samples is compared to the reflections present for references as given by the database used by the X'Pert HighScore Plus software. The comparison of the reflection pattern of the samples with that of cubic pyrite is shown here. The crushed pyrite was obtained from a large crystal cluster; the Boom Clay pyrite was isolated by flotation from Boom Clay.

of bacterial colonies (Vandenberhge et al., 2014; Ostwald and England, 1979). EDX results of five point measurements showed an at% Fe/S ratio of 0.5 ± 0.1, which was lower than for crushed pyrite but is in line with the pyrite stoichiometry (theoretical Fe/S at% ratio = 0.5).

3.1.2. Mineralogy by XRD

The X-ray diffractogram and reflection pattern (Fig. 2) showed that the crystalline material in the bulk of a crushed pyrite sample was indeed pyrite, mostly cubic (with perpendicular axes) in form. XRD is a bulk technique that cannot identify small amounts of minerals present (typically less than 5% of the total mass of the sample). This can explain why no quartz was observed in the XRD measurements, while about 1% of Si was observed in SEM-EDX. Residual reflections for the pattern of crushed pyrite at 43.5 and 44.5°2θ, indicated with a blue rectangle in Fig. 1, could not be identified. This is in fact a broad peak between 43 and 45°2θ. As such, it is hypothesized to be nano-sized cubic iron, which shows reflections at 44.354, 64.528 and 81.657°2θ. Since peak broadening increases with smaller crystal sizes, this cubic iron might be present as (part of) the nanoparticles observed with SEM.

The XRD pattern for the Boom Clay pyrite again showed that pyrite was the only crystalline material found in the bulk of the sample. One reflection of the XRD pattern could not be associated with any mineral (indicated with a green rectangle in Fig. 2). As shown in the diffractogram, the reflection is situated around 26 °2θ and is narrow, implying this is not related to very small crystalline domains (or very small nanoparticles) nor to pseudo arrangement. Only cubic pyrite could be associated to the rest of the pattern. As observed in SEM-EDX, this pyrite consists of mainly framboidal pyrite and some large (5–10 μm) cubic crystals. Both the larger cubic crystals and the framboidal pyrite clusters can be associated to the cubic pyrite reflection pattern. These framboids may likely exhibit a high degree of ordered structures displayed by the internal microcrystals, in which the morphological orientations of each microcrystal appear to be uniform, in the form of cubic-close packing (Ohfuji et al., 2006).

3.1.3. Specific surface by BET

Characterization by BET analysis determined that the specific surface area of the crushed pyrite (after treatment according to Section 2.1.1) was 1.5 ± 0.2 $m^2\ g^{-1}$ (uncertainty based on Student's T distribution with n = 7 and for 95% probability). For Boom Clay pyrite (determined after treatment according to Section 2.1.2), the measured specific surface was comparable at 1.4 ± 0.1 $m^2\ g^{-1}$ (uncertainty based on Student's T distribution with n = 9 and for 95% probability).

For comparison, specific surfaces of cubic pyrite from literature obtained by N_2 adsorption BET measurements show quite some variation depending on the grain sizes, around 1 $m^2\ g^{-1}$ (De Donato et al., 1993), 0.4 $m^2\ g^{-1}$ (Sasaki et al., 1995) and even as low as 0.06 $m^2\ g^{-1}$ (Descostes et al., 2010). For the crushed pyrite studied here however, it is likely that the very small particles, observed in SEM-EDX, contribute to this rather high specific surface area value. For framboidal pyrite, the theoretical maximum specific surface area of a population of 5 μm framboids, assuming all surfaces are available, is 10 $m^2\ g^{-1}$ according to Wilkin et al. (Wilkin and Barnes, 1997). For the Boom Clay pyrite used in the batch tests, larger cubic pyrite crystals were also present, with a smaller specific surface area, leading to an average of 1.4 $m^2\ g^{-1}$.

3.1.4. Surface composition by XPS

The XPS results of both powders, before the start of the batch tests, are shown in Fig. 3. XPS analysis was done at three points for each type of pyrite. One of the spectra is shown in Fig. 3; the others were similar. The relevant contributions of the oxidation states are also indicated on the XPS spectra.

For the iron species, the envelop was decomposed first with a narrow contribution around 707.5 eV that can be assigned to FeS_2 species (Mitchell et al., 2021). The broad part toward higher binding energies observed for both powder types is probably related to other Fe(II) species, such as oxide forms, and maybe to Fe(III) species. Complex multiplet decomposition was applied to simulate the presence of both Fe (II) and Fe(III) oxides according to (Grosvenor et al., 2004) and (Biesinger et al., 2011). For the crushed pyrite, this led to proportions of around 30% of Fe(II)-S, 65% of Fe(II)-O and a possible presence of some Fe(III)-O species. For Boom Clay pyrite, the decomposition of $2p_{2/3}$ bands of this pyrite type is similar to that of the crushed pyrite from the large pyrite cluster, although a much higher contribution of Fe(II)-S, estimated around 55%, and of Fe(II)-O, around 42% was observed. Traces of Fe(III) cannot be excluded for the Boom Clay pyrite either, as well as some Fe(II)-CO_3 species. The corresponding C 1s peak (not shown) indeed suggests the presence of some carbonates for Boom Clay

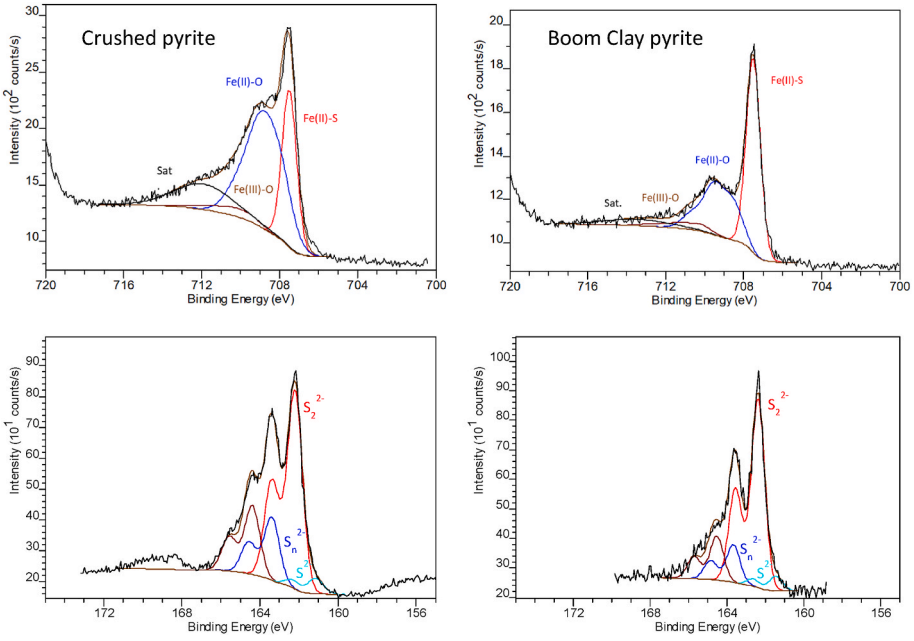

Fig. 3. XPS spectra related to Fe-compounds (top) and S-compounds (bottom) for the crushed pyrite (left) and *Boom Clay* pyrite (right). The deconvolution of the peaks shows the different types of Fe- and S-compounds, as indicated on the graph.

pyrite. Alternatively, this C 1s peak might be related to the presence of surfactant stemming from the extraction process (Section 2.1.2) or kerogen, which is known to be closely intertwined with pyrite in Boom Clay (Bruggeman and De Craen, 2011). The presence of this kerogen may also be the reason why the specific surface area is smaller than expected. Finally, a broad peak satellite centered at 712 eV had to be added to fit the envelope correctly. This peak satellite was difficult to assign. This could be due to some "surface effect" or to interaction of iron with other moieties, i.e., hydroxyl, carbonate, sulfate groups, or a mix of these.

Due to lower split value for the S 2p doublet, each sulfur chemical state could be simulated due to its characteristic doublet shape with the distance between S $2p_{3/2}$ and S $2p_{1/2}$, fixed at 1.18 eV and their ratio kept as 2:1. Mitchell et al. (2021) evidenced many S species that can also be encountered here. For crushed pyrite, the major contribution (57%) was attributed to sulfide related to pyrite with binding energy close to 162.2 eV. Polysulfides (163.2 eV) and elemental sulfur (164.2 eV) could also be suspected but the latter could be confused with thiosulfates or other slightly oxidized sulfur moieties. It was not possible to undoubtedly confirm the presence of sulfates for crushed pyrite, due to the possible contribution of a broad Si 2s energy loss peak (Si presence was indeed also confirmed by SEM-EDX), but sulfates might be present. The S 2p envelop for the Boom Clay pyrite was decomposed similarly to that of crushed pyrite. The major contribution (66%) was again attributed to sulfide related to pyrite, at a higher proportion than for the crushed pyrite, at 66%. The presence of sulfates could be excluded for the Boom Clay pyrite despite the narrower region recorded.

Overall, these XPS results show that the surface of crushed pyrite is quite oxidized (even after HCl treatment), with the presence of mostly Fe (II) oxides in addition to pyrite. Just over half of the sulfur present on the surface could be attributed to pyrite (57% for crushed and 66% for Boom Clay pyrite), while the remainder could not be attributed to oxidized sulfur compounds with certainty. Boom Clay pyrite has a less oxidized surface than crushed pyrite, even though it remains partially oxidized.

3.2. Reactivity of pyrite with nitrate/nitrite

The reactivity of pyrite was evaluated based on the formation of the reaction products in solution (dissolved iron, (thio)sulfate, reduced N species), in Section 3.2.2. The results are reported in mmol per m^2 pyrite, as to normalize for the surface reactive sites of both types of pyrite and to be able to account for small variations in the amount of pyrite added to each replicate. The analysis of the pyrite surface is then discussed in Section 3.2.3. This input is used to hypothesize the reaction pathways between pyrite and nitrate or nitrite in Section 3.2.4.

Since both pyrite starting materials showed a rather oxidized surface, an additional test was done to assess if the oxidized surface would protect the pyrite against any oxidation processes. To this end, 5 g crushed pyrite powder was suspended in 300 mL demi water at room temperature, and was stirred continuously in a glass beaker, open to the air. This allowed for an efficient contact between pyrite and oxygen. The water loss due to evaporation was gravimetrically determined twice per week, and deionized water was added accordingly. Crushed pyrite was chosen as this pyrite type showed the most extensive oxidation of the surface, according to the XPS results. The oxidation was followed up for nearly two months and resulted in a sulfate production of 5.5 $\pm$ 0.31 mmol per m^2 pyrite (supplementary information). This corresponded to the oxidation of 16 mol% of the total pyrite present in the suspension (assuming 100% pure and non-oxidized pyrite at the start) and to a sulfate formation rate of 0.08 $\pm$ 0.01 mmol per m^2 pyrite per day. Thiosulfate was also measured but was always below the detection limit of 1.5 x 10^{-3} mmol per m^2 pyrite. This could be explained by the fact that thiosulfate is an intermediate sulfur species that is readily reduced to sulfate in oxic conditions (Evangelou, 1995). This test showed that the pyrite, even though the surface is rather oxidized, is still very much prone to oxidation and gave a good insight in how a strong oxidant, oxygen, reacts with pyrite.

3.2.1. Background concentrations

Blank samples were included in the batch tests presented in this paper, to assess the background concentrations of the analyzed components in the pyrite suspensions in bicarbonate solution. Though nitrate or nitrite was never detected in these samples, some of the blanks did contain low concentrations of ammonium for the samples taken between 3 months and 1 year. These concentrations never exceeded 2 x 10^{-2} mM, which was overall very low and close to the detection limit which varied between 1 x 10^{-2} and 1.5 x 10^{-2} mM. Since the ammonium background (shown in supplementary information) was comparable for all cases, with and without nitrate or nitrite, it is not considered as a reaction product of nitrate or nitrite reduction by pyrite.

The gas phase was analyzed for its N_2O and N_2 concentration, the latter only for the test cases with Boom Clay pyrite (tests no. 8–13 in Table 1). The blank sample of Boom Clay pyrite replicate a (test no. 8 in Table 1) was used to determine the background concentration of these gasses. N_2O remained under the detection limit (3 x 10^{-3} mmol per m^2 pyrite). The background concentration of N_2 was 2 $\pm$ 1 x 10^{-2} mmol per m^2 pyrite, based on the N_2 measurements in the blank samples at the start, after 1 month, 3 months and in the final sampling after 2 years (supplementary information). Even though care was taken to avoid N_2 contamination in the samples with Boom Clay pyrite (see Section 2.3), N_2 was thus present in rather high background concentrations, likely as some N_2 was present in the glove box at the start of the batch tests.

Fig. 4 shows the concentrations of the possible pyrite oxidation products (iron, sulfate and thiosulfate) that were measured in the solution of all blank samples.

The blank samples of crushed pyrite showed a very low, rather constant concentration of thiosulfate, which was slightly higher than the detection limit at some sampling times, while the thiosulfate concentrations of the blank samples for Boom Clay pyrite did not exceed the detection limit of 1.5 x 10^{-3} mmol per m^2 pyrite. The low background concentration of thiosulfate in the blanks with crushed pyrite suggests that a small amount of thiosulfate was already present at the surface of the crushed pyrite at the start of the experiment. XPS results in the sulfur binding area of the starting material (Fig. 2) showed a possible contribution of thiosulfate at 164.2 eV. This thiosulfate has most likely leached from the surface upon immersion in the bicarbonate solution.

Sulfate was also present in the blank suspensions of crushed pyrite, at a low and rather constant concentration of about 2 x 10^{-3} mmol per m^2 pyrite throughout the test. The blank samples of Boom Clay pyrite however showed a slight increase of sulfate with time. The sulfate in solution doubled in concentration during the two years of the experiment, remaining very low again at about 2 x 10^{-3} mmol per m^2 pyrite for the final samplings. XPS analysis of both starting materials (Fig. 2) however did not detect sulfate on the surface, though the presence of sulfates in the spectra may have been masked by the Si peak, at least for crushed pyrite (see Section 3.1.4). Nonetheless, the background concentration of sulfate is present throughout the test for all test conditions. Apparently, some sulfur species on the surface are dissolved readily in the bicarbonate solution and are oxidized to sulfate. This has been observed for oxidation of pyrite by O_2 in bicarbonated solutions as well, where both sulfate and thiosulfate leached into the solution (Descostes et al., 2002). Since oxic pyrite oxidation can occur very fast and even at very low concentrations of O_2, the traces of O_2 present in the glove box at the beginning of the batch tests may have caused some additional oxidation of the pyrite surface, resulting in a slightly increased background concentration of sulfate. To decouple the possible oxidation by trace amounts of oxygen and to understand the contribution of nitrate or nitrite to pyrite oxidation, the amounts of sulfate found in the blank solutions are considered as a background.

The total iron in the blank solutions always remained at a background level of about 10^{-3} mmol per m^2 pyrite (or 6 x 10^{-4} M in solution).

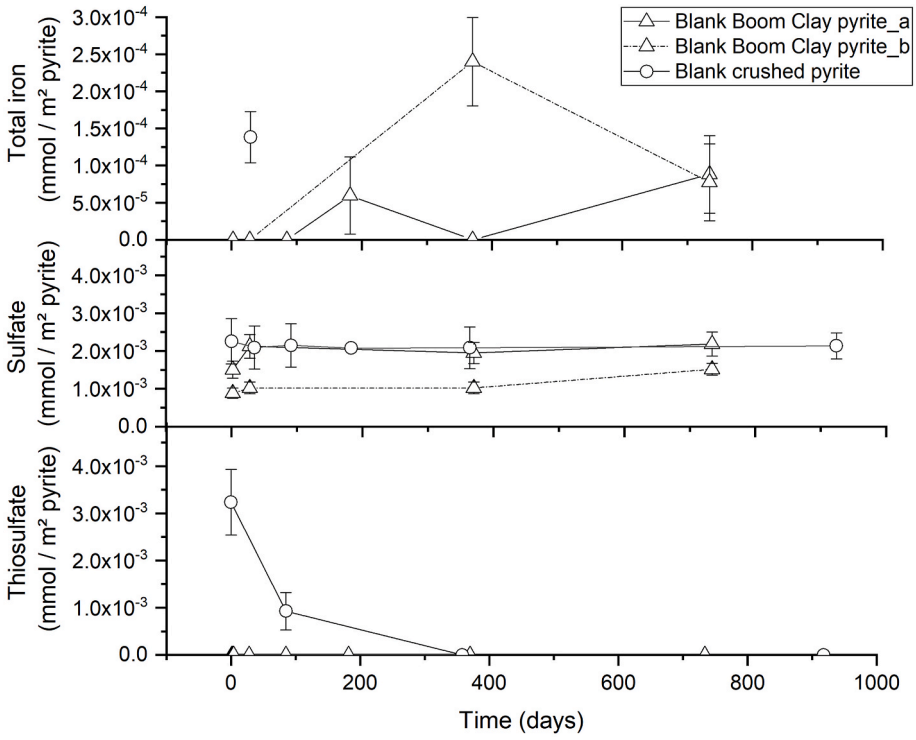

Fig. 4. Average concentrations of total dissolved iron (top), sulfate (middle) and thiosulfate (bottom) measured at different incubation times in blank samples of the pyrite-bicarbonate suspensions, as indicated in the legend: crushed pyrite (test no. 1 in Table 1), and Boom Clay pyrite (test no. 8 and 9 in Table 1). The error bars represent the 95% confidence interval.

3.2.2. *Reaction products in solution*

The nitrate concentration of 0.1 M and 0.005 M, or 14.3 ± 0.6 and 0.72 ± 0.2 mmol per m^2 pyrite, was maintained throughout 2–2.5 years, within the measurement uncertainty. Moreover, iron in solution also remained at the background level of about 10^{-3} mmol per m^2 pyrite and did not increase during the experiments.

Some thiosulfate formation was observed for the crushed pyrite in the presence of nitrate, although this was very low, never exceeding 2 x

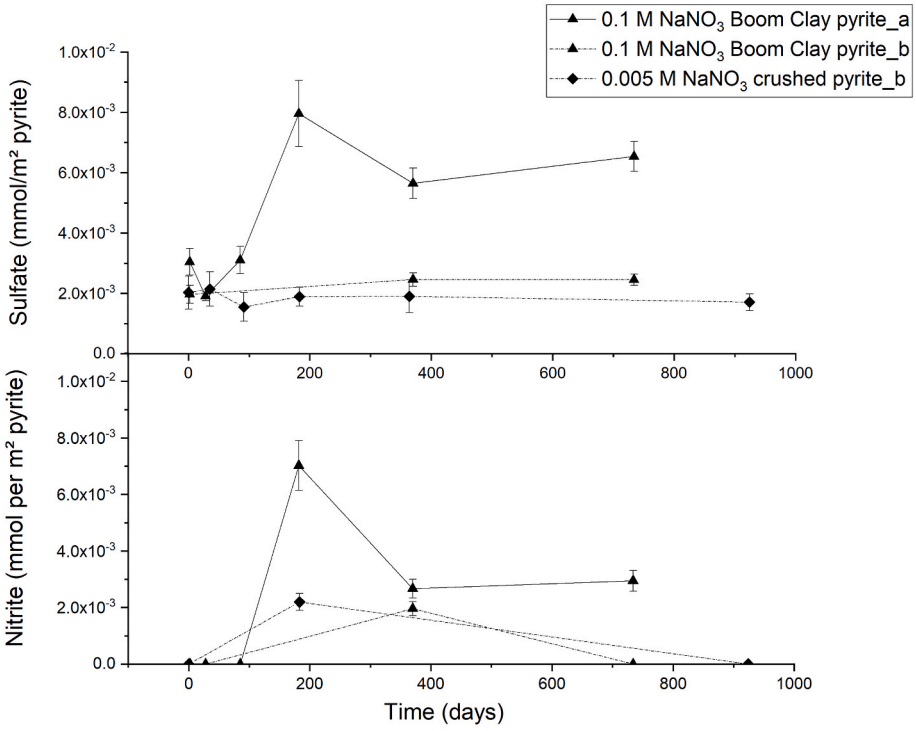

Fig. 5. Concentrations of sulfate (top) and nitrite (bottom) measured at different incubation times in pyrite-bicarbonate suspensions, as indicated in the legend: replicates 'a' and 'b' of the samples with Boom Clay pyrite and 0.1 M $NaNO_3$ (tests no. 10 and 11 in Table 1) and replicate 'b' of the samples with crushed pyrite and 0.005 M $NaNO_3$ (rest no. 3 in Table 1). The error bars represent the 95% confidence interval. The error bars represent the 95% confidence interval.

10^{-3} mmol per m^2 pyrite and remained rather constant in time. Since a similar background concentration of thiosulfate was observed for the blank samples of crushed pyrite (Section 3.2.1), it was not considered in these tests as an oxidation product of pyrite by nitrate. For Boom Clay pyrite with nitrate, thiosulfate concentrations did not exceed the detection limit of 1.5 x 10^{-3} mmol per m^2 pyrite.

The evolution of sulfate was quite similar for the two forms of pyrite in presence of nitrate. For crushed pyrite, the sulfate concentration remained at the background of about 2 x 10^{-3} mmol per m^2 pyrite that was also observed for the blank samples (Section 3.2.1). This was the same for one of the duplicate series ('b') of Boom Clay pyrite, although in the 'a' series, the sulfate concentration increased slightly and exceeded the background level found in the blank samples (Fig. 5). There was a continuous though still very limited production of sulfate during the first 6 months of only this test, after which the sulfate production leveled off. The rather large variation between the two replicates can be a result of the variability of the pyrite powders in the suspensions and the error on the IC measurements. The replicate marked with 'b' could have had a higher degree of oxidation on its surface, causing a slower reaction between nitrate and pyrite. It should be stated that both 'a' and 'b' samples were indeed abiotic according to MPN and ATP microbial activity control tests (supplementary information), confirming that the observed low sulfate production was not the result of a microbial reaction. The observed increase in sulfate concentration did not coincide with an increase of iron in solution.

As only a very slow and limited reaction with pyrite took place based on sulfate concentration evolution, the decrease in the nitrate concentration is smaller than the measurement uncertainty (~5%) and therefore not detected. Nonetheless, some nitrate reduction products were found. Nitrite was detected intermediately for some replicates of both crushed and Boom Clay pyrite (Fig. 6), while it remained under detection limit for the other test cases (supplementary information). The nitrite concentration increased initially, but after 6 months, the concentration decreased again, suggesting that it was formed as an intermediate product. For replicate series 'a' of Boom Clay pyrite, which showed the highest increase in sulfate, the nitrite concentration reaches a maximum value of about 7 x 10^{-3} mmol per m^2 pyrite at 6 months, after which it stabilized at a lower concentration of about 3 x 10^{-3} mmol per m^2 pyrite. This corresponds very well to the sulfate formation observed, since it also increased after 6 months and then stabilized again. The reaction taking place here is likely the incomplete oxidation of pyrite by nitrate, leading to the formation of sulfate and nitrite. For the other replicates, the nitrite concentration decreased to below the detection limit of 3 x 10^{-4} mmol per m^2 pyrite at the end of the test. This can be explained by the further reduction of nitrite with pyrite, a reaction that occurs more rapidly than the reaction with nitrate, as shown in Section 3.2.4.

N_2O was not detected in the gas phase (detection limit is 3 x 10^{-3} mmol per m^2 pyrite), while N_2 remained close to the background in the septum bottles (between 2 and 4 x 10^{-2} mmol per m^2 pyrite, only measured for tests with Boom Clay pyrite).

In the batch tests with Boom Clay pyrite and nitrite, the nitrite concentration of 0.05 M or 7.1 ± 0.3 mmol per m^2 pyrite did not decrease significantly in time, but a clear abiotic reaction was nonetheless observed. For crushed pyrite, a lower nitrite concentration was applied of 0.005 M or 0.66 ± 0.29 mmol per m^2 pyrite, which did decrease with time to 0.44 ± 0.09 mmol per m^2 pyrite for replicate 'a' and 0.45 ± 0.09 mmol per m^2 pyrite for replicate 'b' (Fig. 6). A clear abiotic reaction between pyrite and nitrite can be observed through the increase of both thiosulfate and sulfate concentrations in time, as well as dissolved iron in some cases. Fig. 7 shows the evolution of these dissolved species over time.

More sulfate was found for Boom Clay pyrite than for crushed pyrite, which can be expected since a higher nitrite concentration is applied for Boom Clay pyrite. Note that the produced sulfate concentrations of the replicate series 'a' and 'b' are quite comparable for both pyrite types.

Thiosulfate was also formed in the pyrite suspensions with nitrite, as seen in Fig. 7. For crushed pyrite, double the amount of thiosulfate was formed as compared to sulfate, at a rate of 3.8 x 10^{-5} mmol per m^2 pyrite per day. The amounts formed for replicates 'a' and 'b' are again very

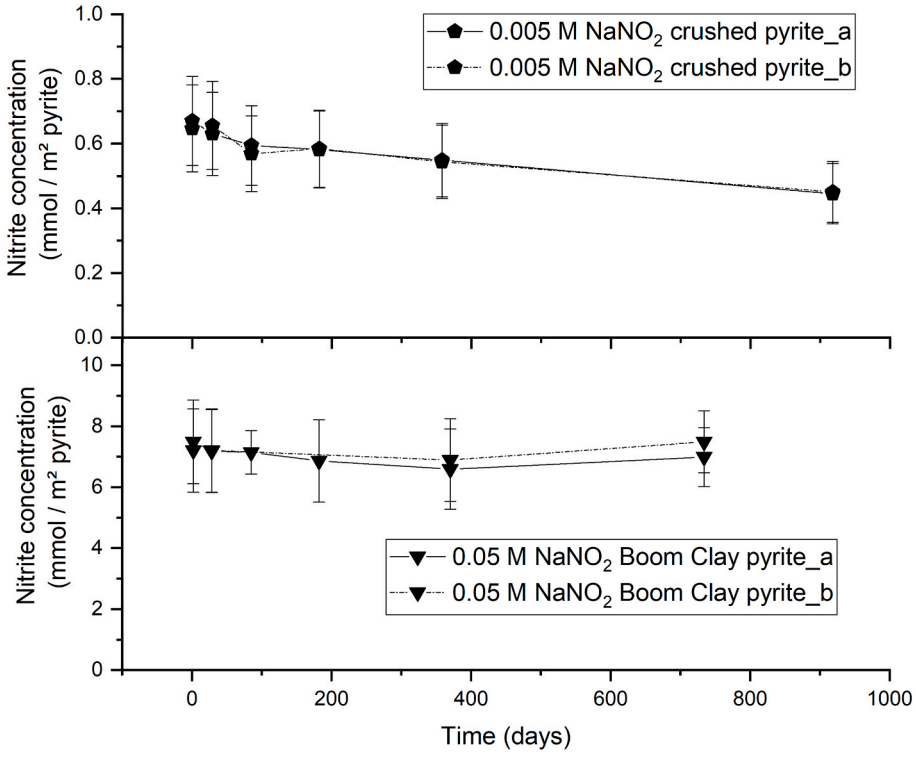

Fig. 6. Average concentrations of nitrite measured at different incubation times in crushed pyrite with 0.005 M $NaNO_2$ (test no. 6 and 7 in Table 1), and Boom Clay pyrite with 0.05 M $NaNO_2$ (test no. 12 and 13 in Table 1). The error bars represent the 95% confidence interval.

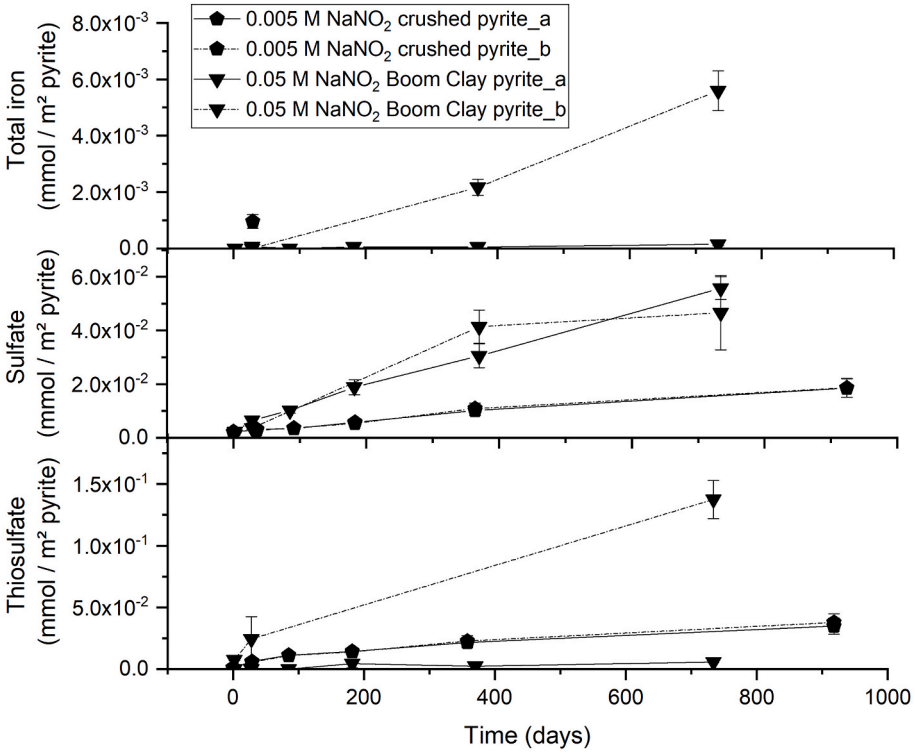

Fig. 7. Average concentrations of total dissolved iron (top), sulfate (middle) and thiosulfate (bottom) measured at different incubation times in various pyrite-bicarbonate suspensions, as indicated in the legend: crushed pyrite with 0.005 M $NaNO_2$ (test no. 6 and 7 in Table 1), and Boom Clay pyrite with 0.05 M $NaNO_2$ (test no. 12 and 13 in Table 1). The blank samples without $NaNO_3$ are also shown for crushed pyrite (test no. 1 in Table 1) and Boom Clay pyrite (test no. 8 and 9 in Table 1). The error bars represent the 95% confidence interval.

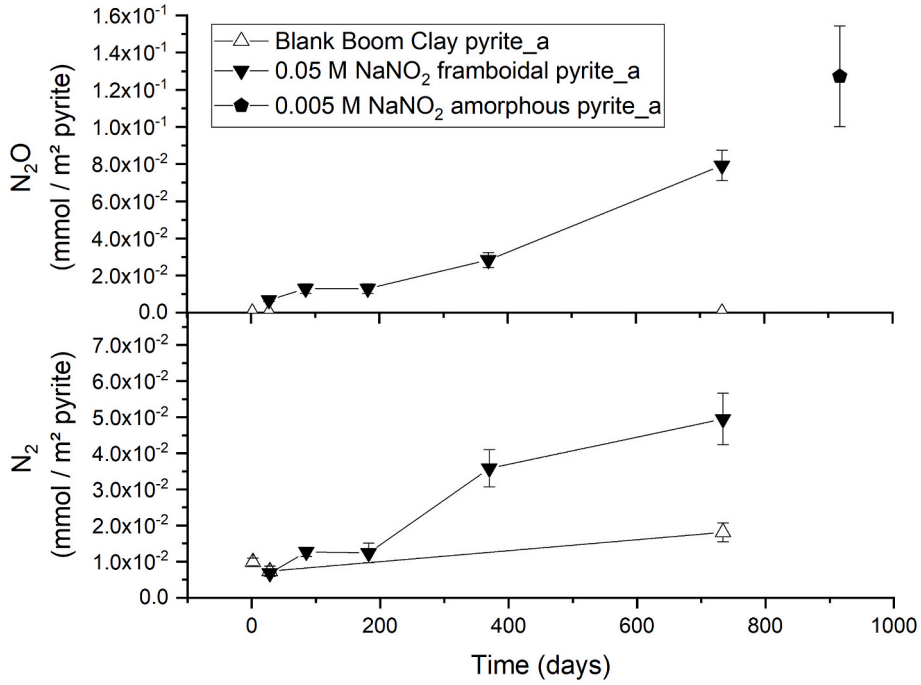

Fig. 8. Average concentrations of N_2O (top) and N_2 (bottom) in the septum bottle, measured after different incubation times in pyrite suspensions in bicarbonate with 0.005 M $NaNO_2$ for crushed pyrite (test no. 4 in Table 1), 0.05 M $NaNO_2$ for Boom Clay pyrite (test no. 12 in Table 1), as indicated in the legend. The blank sample is also shown for Boom Clay pyrite (test no.8 in Table 1). The error bars represent the 95% confidence interval.

comparable. For Boom Clay pyrite, only a limited amount of thiosulfate was formed for replicate 'a'. For replicate 'b' however, twice as much thiosulfate is formed as compared to sulfate. This again shows the inhomogeneity of the pyrite suspensions, especially for Boom Clay pyrite (as also observed for its reactivity with nitrate).

The concentration of iron in solution was only measured after 1 month for the samples with crushed pyrite, which showed an elevated iron concentration in presence of nitrite, as compared to the blank. For Boom Clay pyrite, dissolved iron was measured for each sampling time. It increased strongly in the 'b' series with Boom Clay pyrite (test no. 13 in Table 1), while for the 'a' series the iron remained at or close to the background level found in the blank samples (see Section 3.2.1, Fig. 4).

Note that much less iron was found in solution than expected based on the formation of sulfate and thiosulfate. This can be explained by the solubility/precipitation equilibrium of iron. Indeed, iron can precipitate onto the pyrite surface or reside there in an oxidized form, implying that not all iron that is released from the pyrite through oxidation will be measurable in solution (Murphy and Strongin, 2009).

Since nitrite reacted with pyrite, nitrite reduction products were also expected to be present in the system. In the gas phase, N_2O was detected, more or less at a similar rate for both pyrite forms, as shown in Fig. 8. It should however be noted that this was only measured for the replicate 'a' of all tests, and for crushed pyrite only for the final sampling. N_2 was measured for the samples with Boom Clay pyrite, but again only for the 'a' replicate due to logistical reasons, while a higher iron and thiosulfate concentration was observed for replicate 'b', indicating a stronger reaction here. It should however again be noted that a rather high N_2 background of $2 \pm 1 \times 10^{-2}$ mmol per m^2 pyrite was found for N_2 (based on blank samples, see Section 3.2.1 and Fig. 8). Over 2 years of reaction, in the case of Boom Clay pyrite, $7.9 \pm 0.8 \times 10^{-2}$ mmol N_2O per m^2 pyrite and $5.0 \pm 0.7 \times 10^{-2}$ mmol N_2 per m^2 pyrite had formed. This corresponds to a nitrite reduction of 2.6×10^{-1} mmol per m^2 pyrite, which is smaller than the overall uncertainty on the nitrite measurement, being 3.0×10^{-1} mmol per m^2 pyrite. This explains why a significant decrease in nitrite could not be observed for Boom Clay pyrite. For crushed pyrite, $1.3 \pm 0.3 \times 10^{-1}$ mmol per m^2 pyrite N_2O was produced after 2.5 years, corresponding to a nitrite reduction of about 2.5×10^{-1} mmol per m^2 pyrite. This calculated value in turn corresponds to the observed decrease in nitrite of $2.2 \pm 0.5 \times 10^{-1}$ mmol per m^2 pyrite. It appears that N_2 is thus not formed or at least in a lower amount that for the Boom Clay pyrite, although uncertainties are rather high.

To gain some perspective on the extent of pyrite oxidation based on products found in solution, the most considerable oxidation reactions by nitrate and nitrite, namely replicate 'a' for nitrate and 'b' for nitrite of Boom Clay pyrite (tests no. 10 and 13 in Table 1 respectively), are compared to the oxidation of pyrite by O_2. For test no. 10 with nitrate, 2.5×10^{-3} mmol sulfate per m^2 pyrite was formed intermediately while no thiosulfate was detected (Fig. 7), corresponding to 0.3 mol% of the total pyrite oxidized in 6 months. For test no. 13 with nitrite, both sulfate and thiosulfate were formed corresponding to a total concentration of about 0.18 mmol sulfur oxyanion per m^2 pyrite in solution, which is an oxidation rate of about 2×10^{-4} mmol per m^2 per day. This accounts for an oxidation of about 3 mol% of the total pyrite powder present. In oxic conditions however, sulfate was formed at a linear rate of 5.5 mmol per m^2 pyrite per day, corresponding to the oxidation of 16 mol% of the total pyrite available, within 57 days (see Section 3.2). This indicates that long-term abiotic nitrate and nitrite reduction by pyrite can be detected, though is very limited and occurs with very slow kinetics.

3.2.3. *Changes in pyrite surface chemistry*

XPS analyses of the pyrite were performed at the end of the tests, being 2.5 years for crushed pyrite and 2 years for Boom Clay pyrite. Note that only the 'a' replicates were analyzed.

The first and most obvious observation was that the XPS spectra of all samples, also the blank samples without nitrate or nitrite, have evolved significantly during the experiment towards a large contribution of carbonates (Fig. 3). Immersion in bicarbonate solution thus altered the surface of the pyrite samples quite profoundly, a phenomenon often found in literature (Descostes et al., 2002; Caldeira et al., 2010; Nicholson et al., 1988, 1990). It was found in various studies that in moderately alkaline conditions such as the one presented in this work, soluble iron-carbonate complexes can coexist with pyrite, such as $FeHCO_3^+$, $FeCO_3^0$, $Fe(CO_3)(OH)^-$ and $Fe(CO_3)_2^{2-}$ (Caldeira et al., 2010).

Nonetheless, some interesting observations on nitrate and nitrite reactivity could be made based on XPS results.

Fe $2p_{3/2}$ spectra have evolved significantly from mainly pyrite (A1 and B1 spectra) towards other species due to reactivity with nitrate and bicarbonate (A2 and B2), nitrite and bicarbonate (A3 and B3) and bicarbonate alone (B4). Regarding the detection of carbonates and sulfates on respective C 1s and S 2p spectra, two supplementary multiplet envelopes were added to simulate the presence of iron carbonate (Biesinger et al., 2011) and iron sulfate (Grosvenor et al., 2004). Due to its complexity, such a decomposition has to be considered with caution, particularly for the relative proportion of both of these newly added moieties as their shapes and positions are very similar. Only the carbonates could be confirmed with more certainty, due to a specific contribution detected around 716.0 eV. Furthermore, carbonates were quantified with significantly higher levels (~5%) than sulfates (~1%).

The samples with nitrite (spectra A3 and B3) showed a more pronounced iron carbonate peak at 712 eV compared to the samples with nitrate (spectra A2 and B2). This can be explained by the fact that nitrite effectively oxidized pyrite, thereby releasing Fe(II), which in turn reacts with carbonate in solution and precipitates onto the surface (Descostes et al., 2002). For crushed pyrite in presence of nitrite (A3), an increase in $FeSO_4$ on the surface was found as well, which was not found with nitrate (A2). This could also be linked to pyrite oxidation by nitrite. As shown in Fig. 7, sulfate increased in solution for all samples with nitrite, while this was not the case for the samples with nitrate. Also for the blanks (Section 3.2.1), the initial sulfate release from the surface was higher for crushed pyrite. This was in agreement with the increased sulfate content on the surface. This shows the effect of the origin of the pyrite and the initial surface oxidation on the end products in solution.

When considering the XPS results in the region of the sulfur species (bottom graphs in Fig. 9), the results for bicarbonate solutions with nitrate (A2 and B2), nitrite (A3 and B3) and without nitrogen species (B4) are quite comparable. It is clear that sulfate is formed on the surface of all pyrite samples after 2 or 2.5 years of incubation in bicarbonate solution, in presence and absence of nitrate and nitrite. This can be seen from spectrum B4, of Boom Clay pyrite in bicarbonate solution after 2 years. It thus appears that sulfate is formed simultaneously with the formation of iron carbonates, through the reaction between pyrite and carbonate in the solution. Crushed pyrite had a higher contribution of the sulfate peak (around 169 eV binding energy) as compared to Boom Clay pyrite. It should be noted that the blank sample of crushed pyrite, incubated for 2.5 years in bicarbonate without nitrate or nitrite, was not analyzed by XPS. For crushed pyrite, it therefore remains unclear whether the observed increase in sulfate at the surface – and the higher amount of sulfate present as compared to Boom Clay pyrite – is due to a reaction with nitrate or nitrite or due to the conditions of the test or analyses. Furthermore, it is also clear that sulfate present on the pyrite surface does not necessarily leach into the solution, as shown by the sulfate peak of the B4 sample.

For both Boom Clay and crushed pyrite with nitrate and nitrite, a similar sulfate peak was observed on the surface, while sulfate had partly dissolved into the solution as well (Fig. 9). Thiosulfate was almost completely absent on the surface of Boom Clay pyrite, while it could be observed on crushed pyrite, after 2.5 years of contact with both nitrate and nitrite. In the starting material of crushed pyrite, however, the thiosulfate concentration was even larger. Thiosulfate was thus already present at the surface of crushed pyrite and dissolved into the solution during the experiment, which explains the background concentration observed in solution and the decrease in thiosulfate on the surface.

Overall, it can be concluded that the XPS results (mainly those focusing on iron species) show that nitrite (A3 and B3 in Fig. 9) alters the surface of pyrite more significantly than nitrate (A2 and B2 in Fig. 9), especially in the case of Boom Clay pyrite. Moreover, the XPS spectra of nitrate treated samples (A2 and B2 in Fig. 9) very closely resemble to the spectra of the blanks after 2 year (B4): this confirms the main role played by bicarbonate in the changes of the samples surfaces, rather than nitrate.

3.2.4. *Overall reaction mechanisms between pyrite and nitrate/nitrite*

Aqueous pyrite oxidation in oxic conditions is known to occur by the following reactions (Chandra and Gerson, 2010):

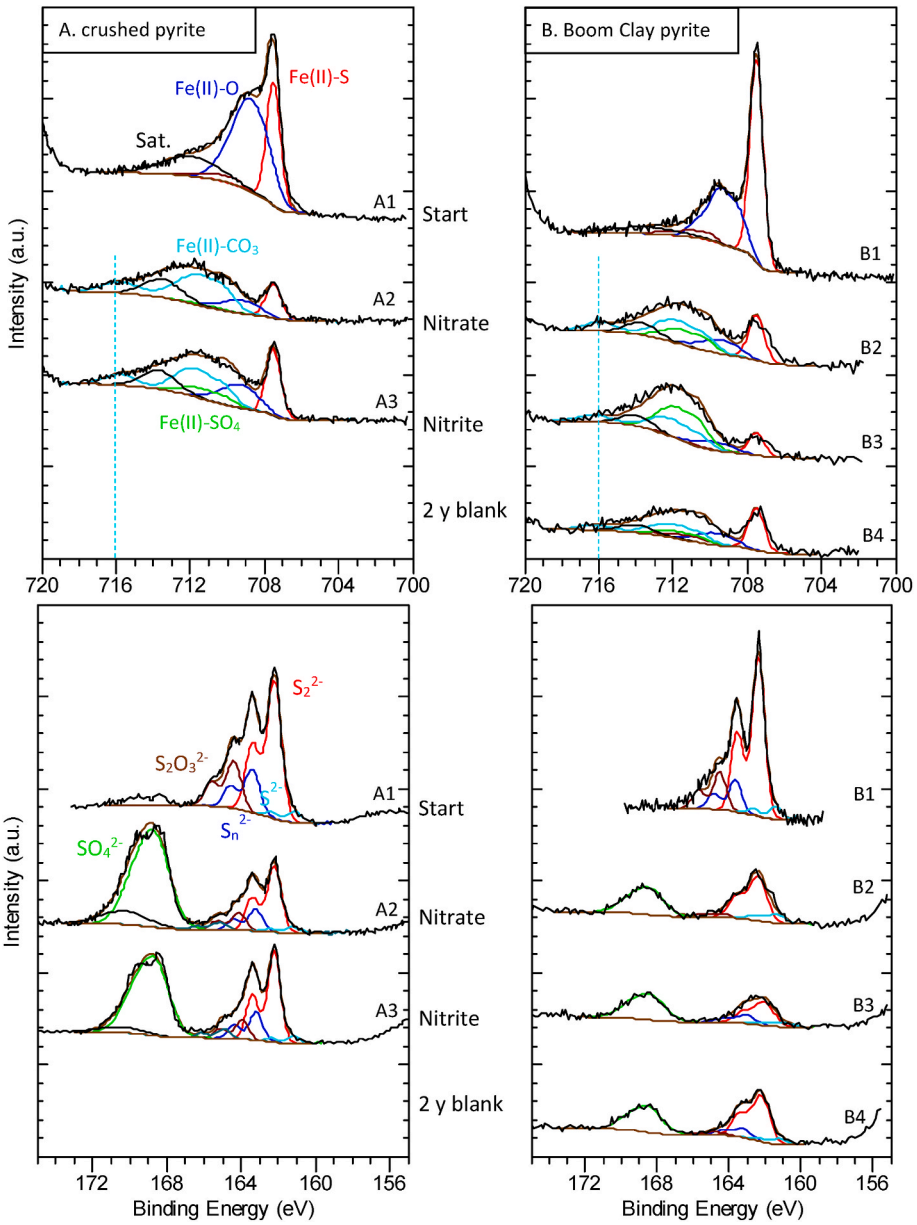

Fig. 9. XPS spectra in the iron (top) and sulfur (bottom) binding region of crushed pyrite (graphs A on the left) and Boom Clay pyrite (graphs B on the right). For crushed pyrite, the pyrite starting material (reported in Section 3.1.4) is shown as spectrum A1, the pyrite after 2.5 years of incubation with 0.1 M nitrate as A2 (no. 2 in Table 1), and with 0.005 M nitrite as A3 (no. 6 in Table 1). For Boom Clay pyrite, the pyrite starting material is shown as spectrum B1 (reported in Section 3.1.4), the pyrite after 2 years of incubation with 0.1 M nitrate as B2 (no. 10 in Table 1), with 0.05 M nitrite as B3 (no. 12 in Table 1) and the blank sample after 2 years in bicarbonate solution as B4 (no. 8 in Table 1).

$$FeS_2 + 7/2\ O_2(aq) + H_2O \rightarrow Fe^{2+} + 2\ SO_4^{2-} + 2\ H^+ \quad (1)$$

$$Fe^{2+} + 1/4\ O_2(aq) + H^+ \rightarrow Fe^{3+} + 1/2\ H_2O \quad (2)$$

$$FeS_2 + 14\ Fe^{3+} + 8\ H_2O \rightarrow 15\ Fe^{2+} + 2\ SO_4^{2-} + 16\ H^+ \quad (3)$$

Fe^{2+} leaches from the surface and sulfates are formed immediately releasing protons and thus causing significant acidification (eq. (1)). With O_2, Fe^{2+} is oxidized to Fe^{3+} (eq. (2)), which is a very potent oxidant of pyrite, forming again Fe(II) and sulfates.

It should also be noted that the carbonates in the solution can react with Fe^{2+}, forming ferrous carbonates (Descostes et al., 2002), which could also explain the ferrous carbonates observed by XPS on the surface of the pyrites (Fig. 9):

$$Fe^{2+} + HCO_3 \rightarrow FeCO_3 + H^+ \quad (4)$$

From the formal reduction potentials (E°') of the redox couples at pH 7, it is clear that nitrate and nitrite are not as strong an oxidant as O_2 and are not oxidants of Fe^{2+}, while O_2 is, as shown in Table 2. Nitrate and nitrite can however oxidize sulfide (to sulfite and further sulfate). It should be noted that these formal reduction potentials are only approximations of the real reduction potentials in the systems with bicarbonate solution. These values were recalculated to pH 7 from their standard reduction potentials, which were expressed compared to the reduction of protons to hydrogen, at pH 0, known as the standard

Table 2
Formal reduction potentials at pH 7 of the relevant redox couples (Liebensteiner et al., 2014).

Redox couple	$E^{0'}$ (V)
$N_2O + 2\ H^+ + 2\ e^- \rightleftharpoons N_2 + H_2O$	1.36
$2\ NO + 2\ H^+ + 2\ e^- \rightleftharpoons N_2O + H_2O$	1.18
$O_2\ (g) + 4\ H^+ + 4\ e^- \rightleftharpoons 2\ H_2O$	0.82
$Fe^{3+} + e^- \rightleftharpoons Fe^{2+}$	0.77
$NO_3^- + 2\ H^+ + e^- \rightleftharpoons NO_2^- + H_2O$	0.43
$NO_2^- + 2\ H^+ + e^- \rightleftharpoons NO + H_2O$	0.35
$HSO_3^- + 6\ H^+ + 6\ e^- \rightarrow HS^- + 3\ H_2O$	−0.11
$SO_4^{2-} + 2\ H^+ + 2\ e^- \rightarrow HSO_3^- + H_2O$	−0.52

hydrogen electrode (SHE). Indeed, the real, in situ reduction potentials are also influenced by the concentrations of the electroactive species present in solution and by other conditions prevailing in solution such as pH, ionic strength, concentration of complexing agents, etc.

Moreover, the reduction of nitrate (full denitrification) occurs in a stepwise reaction through the intermediate formation of nitrite to NO to N_2O and ultimately N_2. It is expected that a similar reaction takes place here. The half reactions of this stepwise reaction are therefore also added in Table 2. The oxidation of pyrite is represented by two half reactions. The oxidation of Fe^{2+} is represented by the Fe^{2+}/Fe^{3+} redox couple, while the oxidation of the sulfide in pyrite to sulfate is represented in the table by the sulfate/sulfide redox couple.

Based on the E°' values of the different redox couples involved, the oxidation of pyrite by nitrate or nitrite, ultimately forming N_2, should indeed be thermodynamically feasible.

In the presence of nitrate, only very limited reactions were observed with Boom Clay pyrite only. This is in line with the fact that, for both types of pyrite, no pH clear changes were observed that would suggest a strong reaction taking place (supplementary information). The bicarbonate solution manages to buffer the production of H^+, if any, in this very slow reaction.

Based on these results, it is not fully understood which reaction takes place between Boom Clay pyrite and nitrate specifically, as iron and sulfur surface chemistry reactions are notoriously complex. Possible reactions in which sulfates are formed, based on oxidation and reduction half reactions and on the reaction products observed in the batch tests with nitrate, are shown in equation (5)–7.

$$FeS_2 + 7\ NO_3^- + H_2O \rightarrow 7\ NO_2^- + Fe^{2+} + 2\ SO_4^{2-} + 2\ H^+ \quad (5)$$

$$4\ FeS_2 + 14\ NO_3^- + 6\ H^+ \rightarrow 7\ N_2O + 4\ Fe^{2+} + 8\ SO_4^{2-} + 3\ H_2O \quad (6)$$

$$5\ FeS_2 + 14\ NO_3^- + 4\ H^+ \rightarrow 7\ N_2 + 5\ Fe^{2+} + 10\ SO_4^{2-} + 2\ H_2O \quad (7)$$

Some literature, mainly research on anaerobic, biotically mediated pyrite oxidation by nitrate, report ferric hydroxide as a reaction product of pyrite oxidation (Bosch et al., 2012). This was however not found here through XPS analysis and is thus not considered.

In all tests with nitrate and pyrite, some intermediately formed nitrite was detected in the duplicates of Boom Clay pyrite, and in one occurrence (one septum bottle) for crushed pyrite (Fig. 5). Since some nitrite was observed, and no N_2 or N_2O was measured above the detection limit or background, we hypothesize that at least eq. (5) occurs when nitrate is in contact with pyrite. This is however a very slow process, especially compared to the oxidation of pyrite in oxic conditions (see Section 3.2.1 and end of Section 3.2.2). It was not possible to verify the stoichiometry of the reaction between nitrate and pyrite. Indeed, the exact amount of pyrite reactive sites could not be measured (uncertainties include the exact surface area, oxidation degree at the start, presence of silica in the case of crushed pyrite and of kerogen intertwined with pyrite in the case of Boom Clay pyrite) and the concentration decrease of nitrate fell within the experimental uncertainty. Additionally, some reaction products, such as dissolved iron, may have precipitated on the surface as Fe(II) minerals such as carbonates, giving an underestimation of the real value of their concentration. Furthermore, based on our results, we cannot exclude nor confirm the occurrence of eqs. (6) and (7), although it is clear that even if they do occur, the reaction rate will be very low.

The produced nitrite concentration declined towards the end of the test for all cases, which is most likely due the faster kinetics of its reaction with pyrite than that of the reaction between nitrate and pyrite, forming said nitrite. Based on the stoichiometry of the half reactions of nitrite reduction and further denitrification (Table 2), this would result in half of the production of N_2 or N_2O up to half of the maximum nitrite concentration observed. Since the background of N_2 was $2 \pm 1 \times 10^{-2}$ mmol per m^2 pyrite and for N_2O the detection limit is 3×10^{-3} mmol per m^2 pyrite, further reduction of the produced nitrite into N_2 or N_2O would likely not have exceeded the N_2 background and N_2O detection limit.

Based on the results of the batch tests with pyrite and nitrite and the above-mentioned further reduction of produced nitrite in the tests with nitrate, nitrite thus also reacted with pyrite, and to a greater extent than nitrate. This difference in reactivity between nitrite and nitrate has been observed for other systems as well, such as the dissolved organic matter of Boom Clay pore water (Bleyen et al., 2016) and the in situ microbial nitrate reduction in Opalinus Clay in a borehole experiment of the Mont Terri rock laboratory (Switzerland) (Bleyen et al., 2018b). The reason for this stronger oxidizing power may be thermodynamic, since nitrite has to recover less electrons than nitrate. Moreover, the reduction of nitrate to nitrite might be the slowest step in the nitrate reduction system ($NO_3^- \rightarrow NO_2^- \rightarrow NO \rightarrow N_2O \rightarrow N_2$), which also explains the faster oxidation by nitrite. For the pyrite suspensions with an initial nitrite concentration of 0.05 M or 0.005 M (which is 100 and 10 times higher respectively than the highest nitrite concentration measured in the tests with 0.1 M $NaNO_3$), sulfate and thiosulfate were the main oxidation products in the solution. Moreover, gaseous N species were found as reduction products of nitrite and the pyrite surface showed oxidized iron sulfate species.

The observed sulfate and thiosulfate production can be the result of the following reaction between pyrite and nitrite:

$$2\ FeS2 + 14\ NO2- + 10\ H+ \rightarrow 7\ N2O + 2\ Fe2+ + 4\ SO42- + 5\ H2O \quad (7)$$

$$3\ FeS_2 + 14\ NO_2^- + 8\ H^+ \rightarrow 7\ N_2 + 3\ Fe^{2+} + 6\ SO_4^{2-} + 4\ H_2O \quad (8)$$

$$FeS_2 + 2\ NO_2^- + 2\ H^+ \rightarrow N_2 + Fe^{2+} + S_2O_3^{2-} + H_2O \quad (9)$$

Since N_2O was produced as well, and for Boom Clay pyrite also N_2 (not measured for crushed pyrite), all proposed reaction pathways are indeed possible. The pH increased somewhat in time (Fig. 10), again making a combination of the above reactions plausible. It was again not possible to verify the exact stoichiometry based on the measured concentrations due to the large uncertainty on the actual reactive surface of the pyrite and the underestimation of the formation of certain species (dissolved iron, sulfur species) that may have precipitated on the pyrite surface. The observed reaction rates for pyrite and nitrite are shown in Table 3.

Based on the observed reaction rates with nitrite, there seems to be a difference in reactivity between crushed and Boom Clay pyrite. However, it is important to note that the nitrite concentration applied for crushed pyrite was 10 times lower than for Boom Clay pyrite, which can cause this lower reaction rate. It is also possible that crushed pyrite has

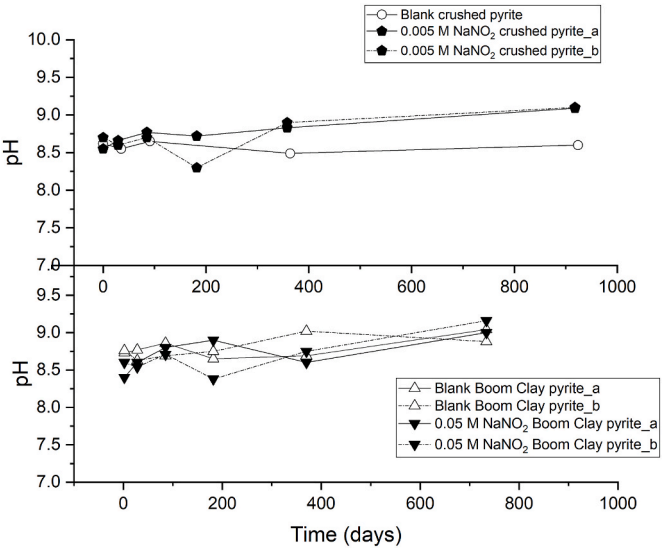

Fig. 10. pH evolution of the tests with nitrite and the blank samples.

Table 3
Production rates based on the final samplings of all test cases with an initial nitrite concentration, together with the results of the blanks. For total iron in the crushed pyrite samples, only one measurement was done after one month and this is given here. The rates are given in mmol per m^2 pyrite per day and the uncertainties on the values are maximally 25% of the reported values. <DL indicates that all values were below detection limit and no rate could be calculated.

Test case	no.	Thiosulfate	Sulfate	Total iron	N_2	N_2O
Blank crushed	1	< DL	Constant background	4.76×10^{-6}	Not measured	Not measured
0.005 M $NaNO_2$ crushed_a	6	3.8×10^{-5}	2.0×10^{-5}	3.3×10^{-5}	Not measured	1.4×10^{-4}
0.005 M $NaNO_2$ crushed_b	7	4.1×10^{-5}	2.0×10^{-5}	Not measured	Not measured	Not measured
Blank Boom Clay_a	8	< DL	3.5×10^{-6}	< DL	< DL	< DL
Blank Boom Clay_b	9	< DL	2.1×10^{-6}	< DL	Not measured	Not measured
0.05 M $NaNO_2$ Boom Clay_a	12	7.9×10^{-6}	7.6×10^{-5}	2.0×10^{-7}	6.7×10^{-5}	1.1×10^{-4}
0.05 M $NaNO_2$ Boom Clay_b	13	1.9×10^{-4}	6.4×10^{-5}	7.6×10^{-6}	Not measured	Not measured
Oxic conditions	/	Not measured	8.1×10^{-2}	Not measured	Not measured	Not measured

less reactive sites due to its more oxidized surface and less contact surface compared to Boom Clay pyrite. XPS results for Boom Clay pyrite (see Section 3.1.4) indeed show that about 66% of the sulfur on the surface was present as disulfide (S_2^{2-}) related to pyrite, while this was 57% for crushed pyrite. The morphology of Boom Clay pyrite also suggests a higher contact surface than that of crushed pyrite, which has less indents than Boom Clay pyrite grains. Overall, the difference between the two types of pyrite is not very large and their reactivity with nitrite is very limited as compared to pyrite oxidation in oxic conditions (at least a factor 3 lower in terms of sulfate generation, Table 4).

For Boom Clay pyrite, a significant difference in reactivity was also observed between the two replicate series 'a' and 'b'. It is not clear what exactly has caused this difference, but a variability in the accessibility of reactive sites at the surface due to variations in oxidation degree or in degree of coverage by organic compounds (closely intertwined kerogen or surfactant residue still adhering to the pyrite surface) is most likely. Boom Clay pyrite seems to be less homogeneous than the crushed counterpart is. This can be the result of the preparation of the pyrite, which in the case of crushed pyrite started from a large, homogeneous pyrite block, while for Boom Clay pyrite it was obtained through various steps from a Boom Clay core containing many different minerals and organic matter.

Overall, the reactivity of the investigated systems could be summarized as indicated in Table 4.

It is important to note that the observed reactions and reaction rates might be an underestimation of the actual processes that could take place in situ, since the pyrite was partially oxidized at the start. Nonetheless, even if there were a one-to-one relationship between available pyrite reactive sites and reaction rates, the actual reaction rates would be more or less double that of the observed reaction rates. This would still be very low for all reactions observed.

4. Conclusions

While the oxidation of pyrite in oxic conditions is rather well understood, the abiotic reaction between pyrite and nitrate or nitrite, studied over multiple years at room temperature and atmospheric pressure, has, to the knowledge of the authors, not yet been studied in detail. A comparison between the reactivity of two types of pyrite with both nitrate and nitrite was made here, in the frame of compatibility studies of Eurobitum radioactive waste and the Boom Clay host rock. Overall, it was clear that the abiotic reactivity between pyrite and nitrate or nitrite is very limited, even when assessed over long periods of time.

Two forms of pyrite from different origin, one from a Peruvian mine in the form of a large pyrite crystal cluster and one extracted by flotation from Boom Clay, were characterized by various techniques. They showed a difference in morphology and surface chemistry. The pyrite powder obtained through crushing of the Peruvian crystal cluster showed very small particles on the surface and an overall crushed morphology. The pyrite obtained from Boom Clay was framboidal and cubic in nature.

In the presence of nitrate, little oxidation of pyrite was observed. For crushed pyrite, no reaction with nitrate was detected in the timeframe of the experiment (2.5 years) in terms of pyrite oxidation products found in solution or decline of nitrate concentration. For Boom Clay pyrite, a very limited reaction between pyrite and nitrate was observed for one of the replicates, forming sulfate and nitrite at comparable rates, both reaching a maximum after 6 months of reaction and subsequently declining in concentration. In the other replicate series, no pyrite oxidation by nitrate was detected.

On the other hand, more reactivity was observed with nitrite compared to the tests with nitrate. Indeed, a limited and slow abiotic reaction was observed between nitrite and crushed pyrite, forming thiosulfate and, to a lesser extent, sulfate (2:1 ratio). In the batch tests with Boom Clay pyrite and nitrite, the sulfate formation occurred twice as fast as for crushed pyrite. However, the variation between the two replicate series with Boom Clay pyrite was again rather large, this time in terms of thiosulfate formation and iron leaching into solution, while the reactions observed for the crushed pyrite replicates were quite comparable. The reaction rates between the two types of pyrite and nitrite were overall quite comparable and quite slow, which was also reflected in the similar XPS spectra observed after reaction with nitrite.

Given the complex nature of the system, hypothetical reaction pathways could be proposed based on the observed reaction products, their stoichiometry and the pH evolution. The proposed reaction pathways included the degradation of pyrite into ferrous ions and sulfate, with nitrate and nitrite being reduced to nitrogen and nitrous oxide gas. However, it was not possible to assess the amount of reactive pyrite sites available for reaction in each case. Moreover, some of the reaction products may have precipitated onto the pyrite surface, leading to an underestimation of the individual, real reaction rates observed.

Overall, the XPS results showed a partial oxidation of the pyrite surfaces at the start of the experiment, which may explain (though only to some extent) the overall slow reaction rates. The Boom Clay pyrite was the least oxidized but also contained some carbon species, which might have been kerogen or surfactant used during the extraction from the Boom Clay. These differences explain the slightly different reactivity for both types of pyrite, although overall comparable reactions were

Table 4
Observed reactions at the end of the batch tests for the test conditions as shown in Table 1. The ratio of the amount of nitrate or nitrite that was added to the test with either crushed or Boom Clay pyrite, is given in the column on the right.

Oxidizing species	Crushed pyrite	Boom Clay pyrite	Concentration ratio NO_x (crushed/Boom Clay)
NO_3^- less reactive species	No reaction detected with **0.1 M** NO_3^- with **0.005 M** NO_3^-	Limited reaction with **0.1 M** NO_3^-	**1/1** **1/20**
NO_2^- more reactive species	Slow reaction with **0.005 M** NO_2^-	Slow reaction with **0.05 M** NO_2^-	**1/10**

observed for both types. Moreover, the XPS analyses suggest that the pyrite surface is largely influenced by the presence of bicarbonate in solution under inert atmosphere, as a large amount of Fe(II)-carbonates was found on the pyrite surfaces in all samples after 2–2.5 years of incubation in 15 x 10^{-3} M sodium bicarbonate solution, the same bicarbonate concentration as in the pore water of Boom Clay. The formation of Fe(II) carbonates at the surface of pyrite in Boom Clay can thus be expected. Such a surface layer may also limit the reaction between pyrite and nitrate and nitrite. Changes of the pyrite surface chemistry due to oxidation by either nitrate or nitrite were very limited, which is in agreement with the limited amount of reaction products found in the solution. Overall, in 0.015 M $NaHCO_3$ solutions (pH ~8.5) and under abiotic, anoxic conditions, nitrate and nitrite do not seem to be very strong oxidizers for pyrite, especially when compared to oxygen.

To extrapolate these results to disposal conditions, two main limitations of the current experimental setup need to be taken into account. Indeed, pyrite will not be freely available as a dispersed powder in clay pore water, but will be embedded in the clay, closely intertwined with kerogen. In the Boom Clay, the reactive surface area is thus expected to be lower compared to in our study. On the other hand, the pyrite embedded in the Boom Clay will not exhibit a partial oxidation of the surface in contrast to the pyrite used in our batch tests. It would thus be very interesting to investigate the availability of pyrite for these types of reactions under in situ conditions, in/with unperturbed Boom Clay.

Declaration of competing interest

The authors declare that they have no known competing financial interests or personal relationships that could have appeared to influence the work reported in this paper.

Acknowledgements

This work was undertaken in close co-operation with, and with the financial support of ONDRAF/NIRAS, the Belgian Agency for the Management of Radioactive Waste and Enriched Fissile Materials, as part of its programme on geological disposal of intermediate-level long-lived waste. The technical assistance of Patrick Boven and Veerle Van Gompel is greatly appreciated, as well as the scientific work of An Mariën and Mirela Vasile on the batch tests described in this paper. The scientific input of Pierre De Cannière and the comments and suggestions of the reviewers are greatly appreciated.

Appendix A. Supplementary data

Supplementary data to this article can be found online at https://doi.org/10.1016/j.apgeochem.2022.105203.

References

Baeyens, B., Maes, A., Cremers, A., Henrion, P., 1985. Aging effects in Boom clay. Radioact. Waste Manag. Nucl. Fuel Cycle 6 (3–4), 409–423.

Biesinger, M.C., Payne, B.P., Grosvenor, A.P., Lau, L.W., Gerson, A.R., Smart, R.S.C., 2011. Resolving surface chemical states in XPS analysis of first row transition metals, oxides and hydroxides: Cr, Mn, Fe, Co and Ni. Appl. Surf. Sci. 257 (7), 2717–2730.

Bleyen, N., Vasile, M., Marien, A., Bruggeman, C., Valcke, E., 2016. *Assessing the oxidising effect of $NaNO_3$ and $NaNO_2$ from disposed Eurobitum bituminised radioactive waste on the dissolved organic matter in Boom Clay*. Appl. Geochem. 68, 29–38.

Bleyen, N., Mariën, A., Valcke, E., 2018a. *The Geochemical Perturbation of Boom Clay Due to the $NaNO_3$ Plume Released from Eurobitum Bituminised Radioactive Waste: Status 2013*, External Report ER-0221. SCK CEN, Mol, Belgium.

Bleyen, N., Smets, S., Small, J., Moors, H., Leys, N., Albrecht, A., Canniere, P.D., Schwyn, B., Wittebroodt, C., Valcke, E., 2018b. Impact of the electron donor on in situ microbial nitrate reduction in Opalinus Clay: results from the Mont Terri rock laboratory (Switzerland). In: Mont Terri Rock Laboratory, 20 Years. Springer, pp. 357–376.

Bosch, J., Lee, K.-Y., Jordan, G., Kim, K.-W., Meckenstock, R.U., 2012. Anaerobic, nitrate-dependent oxidation of pyrite nanoparticles by Thiobacillus denitrificans. Environ. Sci. Technol. 46 (4), 2095–2101.

Bruggeman, C., De Craen, M., 2011. *Boom Clay Natural Organic Matter*, External Report ER-206. SCK CEN, Mol, Belgium.

Bruggeman, C., Maes, N., 2017. *Radionuclide Migration and Retention in Boom Clay*, External Report ER-0345. SCK CEN, Mol, Belgium.

Buresh, R. J. and Moraghan, J., *Chemical Reduction of Nitrate by Ferrous Iron*, 1976. Wiley Online Library.

Caldeira, C.L., Ciminelli, V.S.T., Osseo-Asare, K., 2010. The role of carbonate ions in pyrite oxidation in aqueous systems. Geochem. Cosmochim. Acta 74 (6), 1777–1789.

Chandra, A.P., Gerson, A.R., 2010. The mechanisms of pyrite oxidation and leaching: a fundamental perspective. Surf. Sci. Rep. 65 (9), 293–315.

De Cannière, P., Maes, A., Williams, S., Bruggeman, C., Beauwens, T., Maes, N., Cowper, M., 2010. *Behaviour Of Selenium in Boom Clay*, External Report ER-120. SCK CEN, Mol, Belgium.

De Donato, P., Mustin, C., Benoit, R., Erre, R., 1993. Spatial distribution of iron and sulphur species on the surface of pyrite. Appl. Surf. Sci. 68 (1), 81–93.

Delécaut, G., 2004. The Geochemical Behaviour of Uranium in the Boom Clay. Unpublished, Ph. D. Thesis. Catholic Univ., Louvain.

Descostes, M., Beaucaire, C., Mercier, F., Savoye, S., Sow, J., Zuddas, P., 2002. *Effect of carbonate ions on pyrite (FeS_2) dissolution*. Bull. Soc. Geol. Fr. 173 (3), 265–270.

Descostes, M., Schlegel, M.L., Eglizaud, N., Descamps, F., Miserque, F., Simoni, E., 2010. Uptake of uranium and trace elements in pyrite (FeS2) suspensions. Geochem. Cosmochim. Acta 74 (5), 1551–1562.

Evangelou, V.P., 1995. Pyrite Oxidation and its Control. CRC Press, Inc, Boca Raton, Florida, USA.

Flere, J.M., Zhang, T.C., 1998. Sulfur-based autotrophic denitrification pond systems for in-situ remediation of nitrate-contaminated surface water. Water Sci. Technol. 38 (1), 15–22.

Golez, N.V., Kyuma, K., 1997. Influence of pyrite oxidation and soil acidification on some essential nutrient elements. Aquacult. Eng. 16 (1), 107–124.

Grosvenor, A., Kobe, B., Biesinger, M., McIntyre, N., 2004. Investigation of multiplet splitting of Fe 2p XPS spectra and bonding in iron compounds. Surf. Interface Anal. 36 (12), 1564–1574.

Hendrix, K., Bleyen, N., Mennecart, T., Bruggeman, C., Valcke, E., 2019. Sodium azide used as microbial inhibitor caused unwanted by-products in anaerobic geochemical studies. J. Appl. Geochem. 107, 120–130.

Hunter, W.J., Shaner, D.L., 2010. Biological remediation of groundwater containing both nitrate and atrazine. Curr. Microbiol. 60 (1), 42.

Imai, H., Kawasaki, M., Yamaguchi, M., Takahashi, M., 1985. Mineralization and paragenesis of the Huanzala mine, central Peru. Econ. Geol. 80 (2), 461–478.

Jordan, F., Waugh, W.J., Glenn, E.P., Sam, L., Thompson, T., Thompson, T.L., 2008. Natural bioremediation of a nitrate-contaminated soil-and-aquifer system in a desert environment. J. Arid Environ. 72 (5), 748–763.

Jørgensen, C.J., Jacobsen, O.S., Elberling, B., Aamand, J., 2009. Microbial oxidation of pyrite coupled to nitrate reduction in anoxic groundwater sediment. Environ. Sci. Technol. 43 (13), 4851–4857.

Klueglein, N., Kappler, A., 2013. Abiotic oxidation of Fe (II) by reactive nitrogen species in cultures of the nitrate-reducing Fe (II) oxidizer A cidovorax sp. BoFeN1–questioning the existence of enzymatic Fe (II) oxidation. Geobiology 11 (2), 180–190.

Liebensteiner, M.G., Tsesmetzis, N., Stams, A.J., Lomans, B.P., 2014. Microbial redox processes in deep subsurface environments and the potential application of (per) chlorate in oil reservoirs. Front. Microbiol. 5, 428.

Miller, K., 1974. Flotation of Pyrite from coal.[Removal of Pyrites from Coal by 2-stage Froth Flotation]. U.S. Patent No 3807557.

Mitchell, C.E., Terranova, U., Beale, A.M., Jones, W., Morgan, D.J., Sankar, M., de Leeuw, N.H., 2021. *A surface oxidised Fe–S catalyst for the liquid phase hydrogenation of CO_2*. Catal. Sci. Technol. 11 (3), 779–784.

Murphy, R., Strongin, D.R., 2009. Surface reactivity of pyrite and related sulfides. Surf. Sci. Rep. 64 (1), 1–45.

Nesbitt, H., Bancroft, G., Pratt, A., Scaini, M., 1998. Sulfur and iron surface states on fractured pyrite surfaces. Am. Mineral. 83 (9–10), 1067–1076.

Nicholson, R.V., Gillham, R.W., Reardon, E.J., 1988. Pyrite oxidation in carbonate-buffered solution: 1. Experimental kinetics. Geochem. Cosmochim. Acta 52 (5), 1077–1085.

Nicholson, R., Gillham, R.W., Reardon, E.J., 1990. Pyrite oxidation in carbonate-buffered solution: 2. Rate control by oxide coatings. Geochem. Cosmochim. Acta 54 (2), 395–402.

Ohfuji, H., Rickard, D., Light, M.E., Hursthouse, M.B., 2006. Structure of framboidal pyrite: a single crystal X-ray diffraction study. Eur. J. Mineral 18 (1), 93–98.

Ostwald, J., England, B.M., 1979. The relationship between euhedral and framboidal pyrite in base-metal sulphide ores. Mineral. Mag. 43 (326), 297–300.

Sander, R., 2015. Compilation of Henry's law constants (version 4.0) for water as solvent. J. Atmos. Chem. Phys. 15 (8).

Sasaki, K., Tsunekawa, M., Ohtsuka, T., Konno, H., 1995. Confirmation of a sulfur-rich layer on pyrite after oxidative dissolution by Fe(lll) ions around pH2. Geochem. Cosmochim. Acta 59 (15), 3155–3158.

SCK-CEN, 2020. HADES underground laboratory. Accessed on 22-03-2020; Available from: https://science.sckcen.be/en/Facilities/HADES.

Vaclavkova, S., Schultz-Jensen, N., Jacobsen, O.S., Elberling, B., Aamand, J., 2015. Nitrate-controlled anaerobic oxidation of pyrite by Thiobacillus cultures. Geomicrobiol. J. 32 (5), 412–419.

Vandenberhge, N., De Craen, M., Wouters, L., 2014. The Boom Clay Geology. From sedimentation to present-day occurrence. A review. Mem. Geol. Surv. Belg. 60, 1–76.

Végh, J., 2006. The Shirley background revised. J. Electron. Spectrosc. Relat. Phenom. 151 (3), 159–164.

Weetjens, E., Sillen, X., Valcke, E., 2006. Deep disposal of Eurobitum bituminised waste: scoping calculations of nitrate release. In: Symposium Proceedings. Scientific Basis for Nuclear Waste Management XXIX. Warrendale, United States, pp. 735–742.

Wilkin, R., Barnes, H., 1997. Formation processes of framboidal pyrite. Geochem. Cosmochim. Acta 61 (2), 323–339.
Yan, R., Kappler, A., Muehe, E.M., Knorr, K.-H., Horn, M.A., Poser, A., Lohmayer, R., Peiffer, S., 2019. Effect of reduced sulfur species on chemolithoautotrophic pyrite oxidation with nitrate. Geomicrobiol. J. 36 (1), 19–29.
Yan, R., Kappler, A., Horn, M.A., Peiffer, S., 2021. Towards a standardized protocol for studying chemolithoautotrophic denitrification with pyrite at circumneutral pH. Appl. Geochem., 104995